



# 1 **A novel spectroscopic approach and sampling method for** 2 **ambient hydrogen chloride detection: HCl-TILDAS**

3 John W. Halfacre<sup>1</sup>, Jordan Stewart<sup>1</sup>, Scott C. Herndon<sup>2</sup>, Joseph R. Roscioli<sup>2</sup>, Christoph Dyroff<sup>2</sup>,  
 4 Tara I. Yacovitch<sup>2</sup>, Michael Flynn<sup>3</sup>, Stephen J. Andrews<sup>1</sup>, Steven S. Brown<sup>4,5</sup>, Patrick R.  
 5 Veres<sup>4</sup>, Pete M. Edwards<sup>1</sup>

6 <sup>1</sup>Wolfson Atmospheric Chemistry Laboratories, Department of Chemistry, University of York, Heslington,  
 7 York, YO10 5DD, UK

8 <sup>2</sup>Aerodyne Research, Inc., Billerica, MA, 01821, USA

9 <sup>3</sup>Department of Earth and Environmental Science, Centre for Atmospheric Science, School of Natural Sciences,  
 10 The University of Manchester, Manchester M13 9PL, UK

11 <sup>4</sup>Chemical Sciences Laboratory, National Oceanic and Atmospheric Administration, Boulder, CO, 80305, USA

12 <sup>5</sup>Department of Chemistry, University of Colorado, Boulder, CO 80309, USA

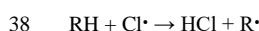
13 *Correspondence to:* John Halfacre ([john.halfacre@york.ac.uk](mailto:john.halfacre@york.ac.uk)), Pete Edwards ([pete.edwards@york.ac.uk](mailto:pete.edwards@york.ac.uk))

14 **Abstract.** The largest inorganic, gas phase reservoir of chlorine atoms in the atmosphere is hydrogen chloride  
 15 (HCl), but the challenges in quantitative sampling of this compound cause difficulties for obtaining high-quality,  
 16 high-frequency measurements. In this work, tunable infrared laser direct absorption spectroscopy (TILDAS) was  
 17 demonstrated to be a superior optical method for sensitive, in situ detection of HCl at the 2925.89645 cm<sup>-1</sup>  
 18 absorption line using a 3 μm interband cascade laser. The instrument has an effective path length of 204 m, 1 Hz  
 19 precision of 7-8 pptv, and 3σ limit of detection ranging from 21-24 pptv. For longer averaging times, the highest  
 20 precision obtained was 0.5 pptv and 3σ limit of detection of 1.6 pptv at 2.4 minutes. HCl TILDAS was also shown  
 21 to have high accuracy when compared with a certified gas cylinder, yielding a linear slope within the expected  
 22 5% tolerance of the reported cylinder concentration (slope = 0.964 ± 0.008). The use of heated inlet lines and  
 23 active chemical passivation greatly improve the instrument response times to changes in HCl mixing ratios, with  
 24 minimum 90% response times ranging from 1.2 - 4.4 s, depending on inlet flow rate. However, these response  
 25 times lengthened at relative humidities > 50%, conditions under which HCl concentration standards were found  
 26 to elicit a significantly lower response (-5.8%). The addition of high concentrations of gas phase nitric acid (>  
 27 4.0 ppbv) were found to increase HCl signal (< 10%), likely due to acid displacement with HCl or particulate  
 28 chloride adsorbed to inlet surfaces. The equilibrium model ISORROPIA suggested a potential of particulate  
 29 chloride partitioning into HCl gas within the heated inlet system if allowed to thermally equilibrate, but field  
 30 results did not demonstrate a clear relationship between particulate chloride and HCl signal obtained with a  
 31 denuder installed on the inlet.

## 32 **1 Introduction**

33 Growing attention is being given to the role of reactive chlorine in tropospheric oxidation chemistry (Simpson et  
 34 al., 2015), given its potential impacts on the lifetimes of volatile organic compounds; atomic chlorine reacts with  
 35 hydrocarbons at rate constants often orders of magnitude greater than those with hydroxyl radical (Burkholder et  
 36 al., 2015; Atkinson et al., 2006; Jahn et al., 2021), as in Reaction (R1), where R represents an alkane:

37



(R1)

39



Even moderate amounts of such a potent oxidizer could lead to changes in concentrations of  $O_3$ ,  $NO_x$ , and hydroxyl radicals. However, the high reactivity of atomic chlorine radicals, combined with a lack of effective gas phase recycling mechanisms, only allows for a small degree of accumulation, with global tropospheric averages estimated to range between  $10^2$ - $10^5$  atoms  $cm^{-3}$  (Allan et al., 2001; Pszenny et al., 2007; Wang et al., 2021; Wingenter et al., 1996; Singh et al., 1996). As such, in situ, quantitative detection of atomic chlorine radicals remains out of reach. It is instead more practical to study chlorine through relatively more abundant and stable reservoir species, such as hydrogen chloride (e.g., Angelucci et al., 2021), molecular chlorine (e.g., Liao et al., 2014), chlorine monoxide (e.g., Tuckermann et al., 1997), and nitryl chloride (e.g., Osthoff et al., 2008).

Hydrogen chloride (HCl) is of particular interest because it is the most abundant form of inorganic chlorine in the gas phase and acts as both a source and end-product of atomic chlorine. Reaction (R1) represents a significant gas phase HCl formation pathway, but its largest atmospheric source on a global basis is sea salt aerosol via acid displacement (Graedel and Keene, 1995, 1996; Wang et al., 2019; Erickson et al., 1999), in which the presence or uptake of other acids, such as nitric acid ( $HNO_3$ ) or even organic acids (Laskin et al., 2012), shifts the equilibrium of aqueous chloride back toward gas phase HCl, as in Reaction (R2) (Brimblecombe and Clegg, 1988; Clegg and Brimblecombe, 1986):



Additional contributions to the HCl budget come from volcanic emissions (von Glasow et al., 2009; Graedel and Keene, 1996) and anthropogenic emissions, including coal combustion, biomass burning, industrial processes (e.g., smelting, cement production), and solid waste incineration (Zhang et al., 2022; Fu et al., 2018; Keene et al., 1999; McCulloch et al., 1999; Ren et al., 2017; Wang et al., 2019). The loss processes for HCl are governed by two major sinks: reaction with hydroxyl radical and deposition. The reaction of HCl with hydroxyl radical in Reaction (R3) directly produces chlorine radicals that can participate in tropospheric oxidation, but is relatively slow ( $k = 7.8 \times 10^{-13}$   $cm^3$  molecule $^{-1}$  s $^{-1}$  at 298 K) (Atkinson et al., 2007):



While deposition of HCl removes a chlorine atom from the gas phase, its eventual uptake into an aqueous solution will produce chloride ions that can be reintroduced into the atmosphere, either by deacidification (as in R2), or via oxidation into other volatile molecular halogens (i.e.,  $Cl_2$ ,  $ICl$ ,  $BrCl$ ) (Abbatt et al., 2010; Fickert et al., 1999; Frinak and Abbatt, 2006; Knipping et al., 2000; Oum et al., 1998) or nitryl chloride (Behnke and Zetzsch, 1990; Behnke et al., 1997, 1992). Recent field observations and modelling suggest the vast majority of tropospheric HCl can be found within 1 km of the surface, with mixing ratios decreasing with height until reaching the tropopause, where mixing ratios begin increasing again (Wang et al., 2019, 2021; Lee et al., 2018; Haskins et al., 2018). In the lower troposphere, ambient HCl mixing ratios are typically observed between  $10^1$  and  $10^3$  parts per trillion by volume (pptv), with the highest amounts found in polluted, coastal regions (Angelucci et al., 2021; Crisp et al., 2014, and references therein; Tao et al., 2022).

Recent technological advances have enabled the production of suitable instrumentation for online, in situ detection of ambient HCl. Chemical ionisation mass spectrometry (CIMS) is one such method, and has been



80 previously characterized in laboratory studies by  $3\sigma$  limits of detection as low as 15 pptv and sensitivities as high  
 81 as 2–4 counts  $\text{sec}^{-1}$  pptv $^{-1}$  (Eger et al., 2019a; Marcy et al., 2004; Roberts et al., 2010). CIMS instruments are also  
 82 robust enough to deploy on mobile platforms, including aircraft (Marcy et al., 2004; Veres et al., 2008) and ships  
 83 (Eger et al., 2019b). The primary disadvantages to CIMS exist in the possibility of sampling compounds (e.g.,  
 84 water) that may interfere with the desired ionisation chemistry (e.g., Marcy et al., 2004), as well as issues of  
 85 selectivity arising from non-analytes that create signal interferences at the desired mass-to-charge ratios meant to  
 86 represent HCl and/or confirm appropriate isotopic ratios and high limits of detection (Eger et al., 2019a; Roberts  
 87 et al., 2010). Additionally, CIMS instruments can be quite heavy, require low vacuums, have high power  
 88 consumption, and often require use of large amounts of consumables (e.g.,  $\text{N}_2$  gas).

89 An alternative, well-understood approach for HCl detection is infrared absorption spectroscopy. Optical  
 90 methods benefit from analysing well-defined and spectrally isolated HCl absorption features (Toth et al., 1970;  
 91 Li et al., 2011), resulting in a virtually absolute and specific measurement technique. Previously published  
 92 literature for laser-based HCl instrumentation has demonstrated potential efficacy for in situ detection, including  
 93 cavity-enhanced (Wilkerson et al., 2021; Hagen et al., 2014; Furlani et al., 2021) and multi-pass cells (Harris et  
 94 al., 1992; Webster et al., 1994; Scott et al., 1999), both of which benefit from path lengths spanning hundreds of  
 95 meters to kilometers. These instruments have also been tested on mobile platforms, such as ships (Harris et al.,  
 96 1992), aircraft (Webster et al., 1994), and balloons (Scott et al., 1999; Wilkerson et al., 2021). The development  
 97 of small, thermoelectrically cooled, interband cascade lasers (ICLs) in recent years has increased the portability  
 98 of these instruments while also allowing the ability to probe the major HCl infrared absorption feature wavelength  
 99 ( $\sim 3.42 \mu\text{m}$ ).

100 CIMS and optical methods have both proven to be excellent means of gas phase HCl detection. However,  
 101 quantitative sampling remains a challenge for all existing measurement techniques. Hydrogen chloride has a large  
 102 dipole moment and strong hydrophilicity, which makes it susceptible to interactions with polar surface groups,  
 103 or surfaces on which water may be present. This “sticky” behavior results in long instrument response times  
 104 during HCl concentration changes (e.g.,  $> 60$  seconds) under sampling configurations that include sample tubing  
 105 and particle filters (Furlani et al., 2021). Further, even inert surfaces, such as those made from  
 106 polytetrafluoroethylene (PTFE) or perfluoroalkoxy (PFA) Teflon, contain sites where HCl or other sticky  
 107 molecules (e.g.,  $\text{HNO}_3$ ) may sorb (Roscioli et al., 2016; Neuman et al., 1999; Yokelson et al., 2003); it has also  
 108 been estimated that PFA Teflon tubing may contain water films between 0.1–10  $\mu\text{m}$  thickness at 20–50% relative  
 109 humidity, which will readily interact with small polar molecules (Liu et al., 2019; Laasonen and Klein, 1997).  
 110 Several coatings have been reported in the literature to improve sticky-compound transmission, including  
 111 halocarbon wax applied to glass (Yokelson et al., 2003; Webster et al., 1994), inert silicon coatings applied to  
 112 stainless steel (Wilkerson et al., 2021), and continual flow of polyfluorinated acid vapor across glass and Teflon  
 113 (Roscioli et al., 2016).

114 In this work, we present a novel optical method for the detection of HCl: Tunable Laser Infrared Direct  
 115 Absorption Spectroscopy (TILDAS), combined with a sampling methodology to minimise inlet artefacts. The  
 116 TILDAS technique has the advantage of being highly sensitive due to its 204 m pathlength, a fast response time  
 117 via incorporation of “active passivation,” and being virtually specific for HCl.



## 118 2 Materials and experimental methods

### 119 2.1 Gases and Chemicals

120 For in-lab experiments, dry air for sample background measurements was generated with an air compressor and  
121 dehumidifying system (dew point approximately  $-60^{\circ}\text{C}$ , absolute water vapor concentration  $\sim 0.01\%$ ). When  
122 testing the effects of water on the sampling configuration in the laboratory, air was manually humidified using a  
123 Michell Instruments DG-3 Dewpoint Generator. This compressed air system was also used in generating nitrogen  
124 ( $\text{N}_2$ ) gas with a commercial  $\text{N}_2$  generator (Infinity NM32L, Peak Scientific Instruments, United Kingdom), which  
125 was used as carrier gas for active passivation (Sect. 2.3) and permeation sources (Sect. 2.4). During field studies,  
126 zero-grade air (270028-L, BOC Limited, United Kingdom) and oxygen-free  $\text{N}_2$  (44-W, BOC Limited, United  
127 Kingdom) were used for these purposes (Sect. 2.5).

128 Perfluorobutanesulfonic acid (PFBS, 97% purity, CAS 375-73-5, Sigma Aldrich, United States) was used  
129 to actively chemically passivate inlet surfaces (Sect. 2.3). Concentrated HCl solution (37% HCl, CAS 7647-01-  
130 0, Fisher Scientific, United States) and concentrated nitric acid ( $\text{HNO}_3$ ) solution (70%, CAS 7697-37-2, Fisher  
131 Scientific, United States) were used in making permeation source standards (Sect. 2.4). A 5 ppm HCl gas cylinder  
132 (diluted in  $\text{N}_2$ , certified as  $4.7\text{ ppm} \pm 5\%$ , 2760716, BOC Limited, United Kingdom) was used as an independent  
133 method validation standard (Sect. 2.4).

### 134 2.2 HCl-TILDAS

#### 135 2.2.1 TILDAS Design

136 The HCl-TILDAS instrument was developed at and purchased from Aerodyne Research Inc (McManus et al.,  
137 2011, 2015). The underlying principle of the tunable infrared laser direct absorption spectrometry (TILDAS)  
138 technique is infrared absorption spectroscopy. Briefly, light from a  $3\mu\text{m}$ -interband cascade laser (operated at  
139  $24.03^{\circ}\text{C}$ ) is collected by an objective, and then is focused through a flip-in pinhole, removed during sampling.  
140 After this focus, the beam is reimaged into the multi-pass, astigmatic Herriott cell. In addition, a beam splitter  
141 enables the laser to travel down a reference path used intermittently to measure and verify the laser tuning rate.  
142 The Herriott cell used in this instrument has an effective path length of 204 m, and is held to a temperature of  $29$   
143  $^{\circ}\text{C}$  by circulating air past temperature controlled liquid along the sides of the instrument (Oasis Model T-Three).  
144 Temperature controlling the interior of the TILDAS mitigates the effects of exterior temperature changes that may  
145 cause optical fringe effects in the reported mixing ratios or changes to the mirror and table distances that may  
146 affect the path travelled by the laser light reaching the detector.

147 This incident radiation probes the strong  $\text{R}(1)\text{H}^{35}\text{Cl}$  line ( $2925.89645\text{ cm}^{-1}$ ) of the (1-0) rovibrational  
148 absorption band near  $3.4\mu\text{m}$  (Guelachvili et al., 1981). The instrument software sweeps the laser over the desired  
149 spectral window, which it can find via strong absorption lines from other spectrally close absorbers, including  
150 methane ( $2926.18\text{ cm}^{-1}$ ,  $2926.700231\text{ cm}^{-1}$ ) and water ( $2926.456\text{ cm}^{-1}$ ,  $2926.742\text{ cm}^{-1}$ ). In addition, the laser is  
151 coincidentally able to estimate concentrations of methanol ( $2925.851\text{ cm}^{-1}$ ,  $2925.998\text{ cm}^{-1}$ ), formaldehyde  
152 ( $2925.842\text{ cm}^{-1}$ ,  $2926.1\text{ cm}^{-1}$ ), and nitrogen dioxide ( $2925.8\text{ cm}^{-1}$ ,  $2926.128\text{ cm}^{-1}$ ). Since the absorbing features in  
153 this region are well-resolved, spectral interferences for HCl are not expected for typical ambient mixing ratios  
154 observed for the above species.

## 2.2.2 Sampling Inlet

Filtration of particulate matter is required to protect and maintain the efficacy of the multi-pass optics described in the previous section (McManus et al., 1995), as well as reduce the potential of scattering and absorption from particulates within the cell. However, traditional paper filters and filter holders provide surfaces onto which HCl may be removed from the sample stream, both lowering the observed concentration and providing a reservoir of HCl that could be later forced back into the gas phase via acid displacement. To obviate this problem, a custom-fabricated quartz virtual impactor (hereafter referred to as “inertial inlet”) was added into the instrument sampling line (Fig. 1). The inertial inlet glass is housed within a temperature-controlled enclosure set to 50 °C (Omega CNI32). Sample air passes from an ambient pressure region through a critical orifice into a low-pressure region (< 100 torr). The resulting flow rate through the instrument was determined by the size of the critical orifice in the inertial inlet and cell pressure (set to approximately 40 torr); because different inlets were used for these experiments, flow rates were 2.8, 3.7 or 12.7 L min<sup>-1</sup>, yielding cell residence times (1/e) of 2.0 s and 1.5 s, and 0.4 s respectively. Once in the low-pressure region, large particles (> 300 nm diameter) have large forward momentum and travel straight into a waste flow path (approximately 13% of the total volumetric flow). Meanwhile, gas molecules and particles with an approximate diameter < 300 nm have less inertia and can make the 180° turn necessary to continue along the sample flow path into the TILDAS (approximately 87% of the total volumetric flow); because the astigmatic Herriott cell used in the TILDAS has a shorter path length / higher light throughput than high finesse cavity systems, it is not as sensitive to decreased light throughput caused by the accumulation of smaller diameter particulate matter on cell mirrors. The inertial inlet is connected to the HCl-TILDAS via 3m of insulated, temperature controlled (50 °C), 3/8” PFA Teflon tubing.

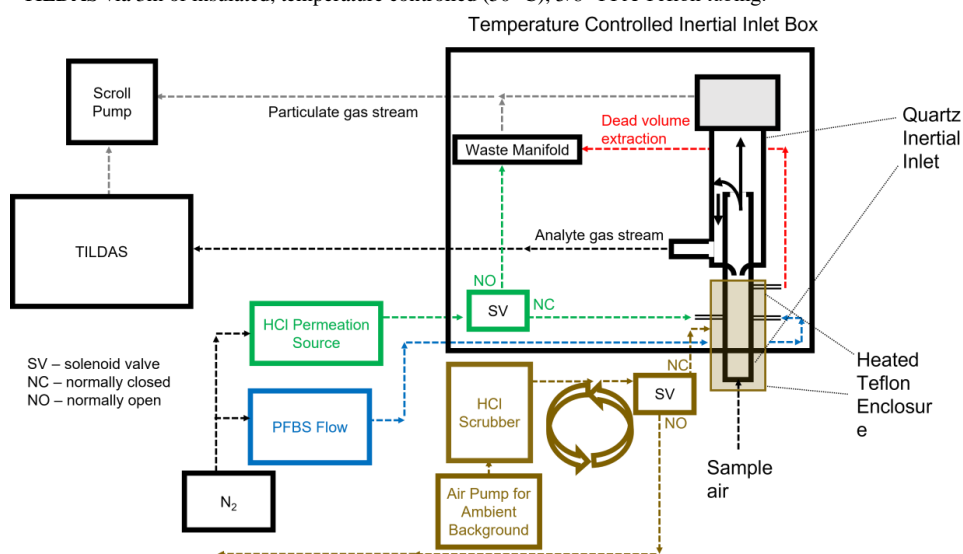


Figure 1: Experimental flow schematic for sampling HCl

## 2.3 Active Passivation

It has been previously shown that adding a small, continuous flow of PFBS vapor to sampling lines is effective at increasing transmission of HNO<sub>3</sub> through sampling tubing (Roscioli et al., 2016). This technique was used in this work to minimize loss of HCl to surfaces between the inertial inlet and the optical cell. Five-mL of PFBS was



180 contained within a bubbler (made from perfluoroalkoxy (PFA) Teflon or Pyrex for laboratory and field studies,  
 181 respectively). Compressed  $N_2$  gas was passed into the bubbler to flush the headspace (containing PFBS vapor)  
 182 into the analyte flow path, just after the point of sample air entry into the inertial inlet (Fig. 1). Addition of fresh  
 183 PFBS vapor into the flow path may quickly release several ppbv of HCl from unpassivated surfaces and may take  
 184 several hours to finish conditioning the system. The temperature and carrier gas flow rate (containing PFBS) were  
 185 adjusted (between 18–22 °C and 50–100 mL min<sup>-1</sup>, respectively) until no additional HCl was released to ensure  
 186 optimal passivation conditions. Given the growing body evidence on the deleterious effects of perfluorinated  
 187 compound accumulation in the environment (Buck et al., 2011), release of PFBS vapor was mitigated by adding  
 188 a scrubber containing hydroxide salts, glass wool, and activated charcoal to the pump exhaust. When replacement  
 189 was necessary, the bubbler and any contaminated tubing were washed with absolute ethanol and fully dried before  
 190 re-use, with rinsings collected and disposed of as hazardous waste.

191 Passivation efficacy was regularly tested as a function of the timescale of signal change resulting from  
 192 the addition / removal of HCl standard flow into the inertial inlet (Fig. 1). Timescales were calculated as detailed  
 193 in Sect. 2.6.2.

#### 194 **2.4 HCl Standards for Technique Validation**

195 Custom HCl permeation sources were created for regular inlet transmission testing using a method modified from  
 196 Furlani et al. (2021). HCl was pipetted into a 2" length of PTFE tubing (0.118" ID, 0.157" OD, VWR). Tubing  
 197 was sealed by heating the ends, one at a time, in a small flame until the tubing became transparent. The end of  
 198 the tubing was then clamped by pliers and removed from the flame, creating a seal on cooling. The completed  
 199 permeation source was then placed in a temperature-controlled aluminum block (set to 35 °C). A flow (30 mL  
 200 min<sup>-1</sup>) of  $N_2$  gas, carries the HCl vapor into the instrument flow path (Fig. 1). Additionally, a permeation source  
 201 for  $HNO_3$  was created and utilized in the same manner for the purposes of studying interferences (Sect. 3.3.2).

202 A cylinder of 5 ppmv ( $4.7 \pm 5\%$ ) HCl (Sect. 2.1) was used to confirm both the TILDAS response to HCl,  
 203 as well as the permeation source output. On opening the cylinder for the first time (or after a period of disuse),  
 204 multiple days of constant flow (controlled between 1–50 mL min<sup>-1</sup> by an Alicat MCS-50SCCM) were required to  
 205 condition the regulator before HCl-TILDAS reflected a stable output. Because TILDAS is an optical method that  
 206 relies on characteristic, well-described absorption features of molecules, it is considered an absolute detection  
 207 method and does not require frequent calibrations.

#### 208 **2.5 Field Testing**

209 To demonstrate its performance as an in situ, field-ready instrument, the HCl-TILDAS was deployed during the  
 210 Integrated Research Observation System for Clean Air (OSCA) campaign at the University of Manchester  
 211 (Manchester, United Kingdom, approximately 53.444 °N, 2.216 °W), and sampled HCl between 10 June - 22 July,  
 212 2021. The OSCA campaign seeks to understand and assess urban air pollution and air quality at various sites  
 213 across the UK in order to inform and support policy makers in making future decisions, as well as evaluating the  
 214 impacts of decisions previously made. More information on the campaign and links to relevant studies can be  
 215 found here: <https://gtr.ukri.org/projects?ref=NE%2FT001917%2F1#/tabOverview>. The measurement site was  
 216 located at the Manchester Air Quality Super Site on the Firs Environmental Research Station at the University of





Manchester campus, and sampled air masses are believed to be heavily influenced by the surrounding urban environment.

The TILDAS instrument and pump for generating background measurements (KNF Model N035.1.2AN.18) were installed within an air-conditioned shipping container, held at 25 °C. The inertial inlet, HCl permeation source, and active passivation unit were integrated into a separate box (80 cm x 60 cm), installed above the container roof (~ 3m AGL) (Fig. 2). Because each of these components are operated at different temperatures (inertial inlet box, permeation source, and active passivant held at 50, 35, and 18 °C, respectively), the larger box was cooled with a water-cooling fan (controlled to 25 °C) to buffer the box interior from changes in the external ambient temperatures and direct solar heating. Temperatures were regularly checked using thermocouples interfaced with an Arduino Uno (Arduino).

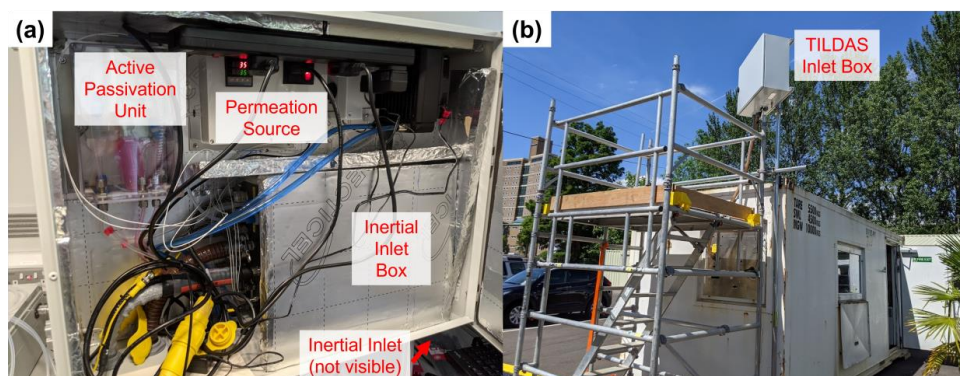


**Figure 2: a) Field configuration for HCl TILDAS inlet system. b) Mounted inlet system at Manchester field site.**

During the campaign, blank measurements were obtained for 2 min out of every 10 min throughout ambient sampling periods in order to check for drifts in instrument background signal due to optical stability. An effective blank was achieved by passing ambient air through a trap composed of activated charcoal and glass wool. This HCl-scrubbed air was then directed to a Teflon encasing around the inertial inlet, which then overflowed the inlet at approximately 35 L min<sup>-1</sup>, such that the inlet would only be sampling scrubbed air. To evaluate the inlet for losses and the efficacy of the PFBS, flow from the HCl permeation source was added directly into the inertial inlet on top of the background air overflow for 9 min every 3 hr. Note that overblows using zero air cylinders were found to cause a large increase in HCl signal, followed by a slow decay; it is believed this is due to the sudden disruption in the equilibrium of water molecules adsorbed to instrumentation surfaces. For this reason, permeation source additions under dry air conditions were performed overnight when ambient HCl chemistry mixing ratios were believed to be low. For these experiments, compressed dry air (produced by Jun Air OF302-25MQ2) overflowed the inlet for 1 hr, and permeation source HCl was added across three 10-min intervals within this hour.

## 2.6 Data Analysis

Data processing for this work, including background corrections and uncertainty analysis, were conducted primarily using the *R* statistical software (R Core Team, 2021) in tandem with the RStudio environment (RStudio Team, 2021).



## 2.6.1 Background Correction

As discussed above, background measurements were obtained for 2 min out of every 10 min sampling period. The median of the final 30s of each background period was used as an offset value. Offset values between these points were estimated by linear interpolation and were subsequently subtracted from ambient observations for analysis.

## 2.6.2 HCl Signal Response Timescales

Timescales of signal decay ( $\tau$ ) after removal of a HCl standard (Sect. 2.4) from the HCl-TILDAS sampling line were calculated as an objective measure of the sampling method performance. Such timescales for sticky gases (including HCl) have been previously determined by fitting data to a biexponential model (Roscioli et al., 2016; Zahniser et al., 1995; Ellis et al., 2010; Pollack et al., 2019):

$$y = A_1 \exp\left(-\frac{t}{\tau_1}\right) + A_2 \exp\left(-\frac{t}{\tau_2}\right) \quad (1)$$

where  $y$  represents the HCl mixing ratio,  $t$  represents elapsed time, both  $A_1$  and  $A_2$  are proportionality terms, and both  $\tau_1$  and  $\tau_2$  control the shape of the decay curve. Herein, both single exponential and biexponential models were fit to the data to determine the time needed to reach  $1/e$  ( $\tau$ ), 75% ( $\tau_{75}$ ), and 90% ( $\tau_{90}$ ) of a starting HCl concentration. The fitting function within  $R$  (i.e., “nls”) required initial guesses for the  $A$  and  $\tau$  terms, which were based on the starting mixing ratio of HCl and anticipated residence time of air in the absorption cell, respectively; however, the function was not constrained to these values in formulating its output.

## 2.6.3 HCl Partitioning

The thermodynamic equilibrium model ISORROPIA II (Fountoukis and Nenes, 2007), used to investigate  $K^+$ – $Ca^{2+}$ – $Mg^{2+}$ – $NH_4^+$ – $Na^+$ – $SO_4^{2-}$ – $NO_3^-$ – $Cl^-$ – $H_2O$  aerosol systems, was employed to estimate the potential that particulate chloride (pCl<sup>−</sup>) may partition to HCl within the heated inlet system. Calculations were performed in ‘forward mode’ when possible, in which the total (gas + aerosol) concentrations of  $NH_3$ ,  $H_2SO_4$ , HCl,  $HNO_3$ ,  $Na^+$ ,  $Ca^{2+}$ ,  $K^+$ , and  $Mg^{2+}$  were specified, alongside ambient temperatures and relative humidities. The model then solves a series of equilibrium equations based on these conditions, incorporating water activity equations, activity coefficient calculations, electroneutrality, and mass conservation, to determine the gas and aerosol concentrations at thermodynamic equilibrium. The calculations were then repeated for different potential TILDAS sample line testing temperatures (35, 50 and 80°C) to determine changes in gaseous HCl mixing ratios resulting from re-partition with aerosols within the sample line. In scenarios where gas phase concentrations were unknown, the model was initialised in ‘reverse mode’ with averaged aerosol concentrations to predict gas phase concentrations at equilibrium. In all model calculations, the aerosol was assumed to be in a thermodynamically stable state, in which salts precipitate if saturation is exceeded, owing to the low relative humidities within the heated inlet line.

## 3 Results & Discussion

### 3.1 Instrument Performance

The performance metrics of HCl-TILDAS are compared with previously described optical methods in Table 1. Allan-Werle deviations were calculated in the laboratory while overflowing the inlet with dry zero air (Sect 2.5)





(Hagen et al., 2014; Furlani et al., 2021), and in the field with HCl-scrubbed sample air (i.e., without removal of water vapor) (Fig. 3). Under 30s integration times and using the 3.7 L min<sup>-1</sup> inlet, the precision (1-2 pptv at 1 $\sigma$ ) and 3 $\sigma$  limit of detection (4-6 pptv) outperform previously reported methods, which range from 6 - 100 pptv precision, and 18 - 78 pptv limits of detection under 30 s averaging times. HCl-TILDAS has clear advantages for both figures of merit if longer integration times are considered; for dry, laboratory conditions, we achieved a precision of 0.5 pptv and corresponding LOD of 1.6 pptv at the Allan minimum of 2.4 minutes, compared with 1.5 pptv precision and 4.4 pptv LOD for field observations at an Allan minimum of 56 seconds. These values are more than adequate for obtaining high quality field observations at the expected ambient HCl mixing ratios of 10<sup>1</sup>-10<sup>3</sup> pptv (Wang et al., 2019).

289

290 **Table 1: Summary table comparing the performance of HCl TILDAS to similar, previously reported optical methods.**  
 291 <sup>a</sup> The lower limit of the figures of merit represent laboratory sampling, while the higher limit represents field sampling.  
 292  $\tau_{90}$  are reported for dry, laboratory sampling conditions. The lower value represents laboratory analysis, while the  
 293 higher value represents data from field work (Fig. 9). <sup>b</sup> Reported for mixing ratio changes > “10<sup>9</sup> per volume or higher”.

Instrument	LOD	Precision	$\tau_{90}$	Reference
HCl-TILDAS <sup>a</sup>	21-24 pptv (1 s) 4-6 pptv (30 s)	7-8 pptv (1 s) 1-2 pptv (30 s)	> 4.4 ( $\pm 0.3$ ) s (2.8 slpm) > 1.15 ( $\pm 0.06$ ) s (12.7 slpm)	This study
Near-IR CRDS	< 18 pptv (30 s)	6 pptv (30 s)	> 10 s	Furlani et al. (2021)
Near-IR CRDS	60 pptv (60 s)	20 pptv (60 s)	10 - 15 s	Hagen et al. (2014)
Off-axis integrated cavity output spectrometer (OA-ICOS)	78 pptv (30 s)	26 pptv (30 s)	10 s	Wilkerson et al. (2021)
Aircraft laser infrared absorption spectrometer (ALIAS)	33 pptv (30 s)	100 pptv (30 s)	10 s <sup>b</sup>	Webster et al. (1994)

294

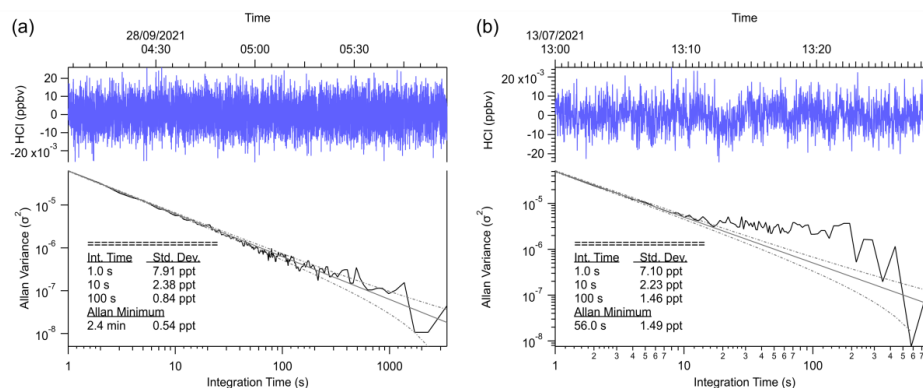


**Figure 3: Allan variance plot demonstrating the signal variance and limit of detection calculations for varying integration times.**

A commercial HCl cylinder with a certified concentration ( $4.7 \text{ ppm} \pm 5\%$ ) was used as an objective standard for in-lab validation. Mixing ratios were varied by adjusting the flow rate of the cylinder output, which was then directly injected into an inertial inlet sidearm (Fig. 1) for direct injection into the passivated inertial inlet. Standard HCl was then diluted into the dry, HCl-free compressed air being sampled by TILDAS. The slope obtained (0.964) was found to lie within the expected 5% uncertainty, reflecting high accuracy for TILDAS observations (Fig. 4). However, additional sources of error causing deviation from unity must be considered. For example, multiple days of HCl cylinder flow are required for the output mixing ratio to stabilize at its maximum concentration (as observed by TILDAS) after opening the cylinder; this behavior is presumably caused by uptake of HCl onto the metal cylinder regulator and Teflon tubing lines until they are fully conditioned, causing the observed signal to register lower than expected. Changes to HCl cylinder flow additionally require similar conditioning time to re-establish signal stability, likely caused by changes to the HCl gas/surface equilibrium.



11

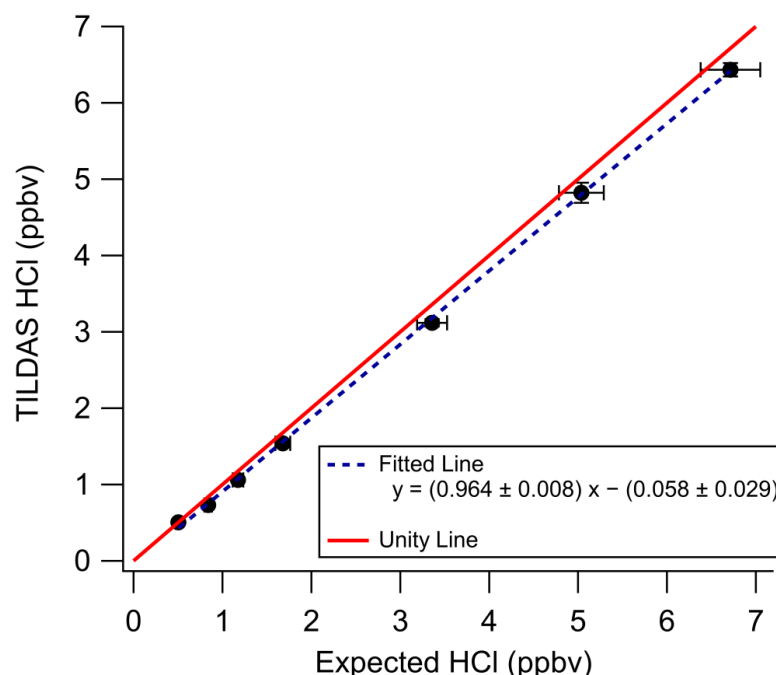


Figure 4: In-lab validation of HCl-TILDAS by a commercial HCl standard. Principal axis error bars represent the 5% uncertainty associated with the HCl standard (as reported by the manufacturer), while the vertical axis error bars represent 1 standard deviation of HCl-TILDAS observations for each validation point.

### 3.2 Evaluation of Sampling Method

Multiple variables were found to affect HCl transmission through the instrument flow path (Fig. 1), including the presence or absence of active passivation (i.e., whether PFBS is flowing through the sample line; Sect 3.2.1) and the presence of water vapor (Sect 3.2.2). The timescales of signal change after removal of an HCl source were used to objectively compare the relative effects of each variable. They further allow for direct comparison of the performance of this HCl sampling method with those previously published (Table 1). Note that these timescales reflect how quickly HCl mixing ratios change within the 1.8L measurement cell and do not include the time required for the sample gas to reach the cell (i.e., time zero is when a change in signal is first observed, not from when an addition valve was triggered).

#### 3.2.1 Active Passivation

To test the effectiveness of active passivation, HCl permeation source flow was added into the TILDAS sample line for 10 min of subsequent 30 min periods using the inertial inlet with the lowest flow rate ( $2.8 \text{ L min}^{-1}$ ), as the effects of HCl-wall interactions would be the most exaggerated. Experiments were repeated both with and without the coinciding flow of PFBS (Fig. 5), and the TILDAS inlet was overflowed with dry, compressed air (Sect. 2.1), such that a baseline signal was observed in the absence of permeation source addition. As seen in Fig. 5a, employing active passivation yields sharp, square wave-like behavior on both addition and removal of the HCl permeation source flow. From the fits of a single exponential model,  $\tau_e$  averaged  $1.9 \pm 0.2 \text{ s}$  ( $N = 21$ ) after HCl



permeation source removal (Fig. 5b, Fig. A1), which compares well with the predicted absorption cell residence time ( $1/e$ ) of 2.0 s. Though a biexponential model was also fit to these data (and achieved comparable  $\tau_e$ ,  $\tau_{75}$ , and  $\tau_{90}$  values, Table A1), the convergence tolerance of the non-linear least squares solving algorithm (Sect. 2.6.2) had to be loosened by six orders of magnitude (from a default value of  $1 \times 10^{-5}$  to  $2 \times 10^1$ ) to achieve convergence, suggesting these results are not meaningful. Indeed, the errors for the predicted variables often greatly exceeded the magnitude of the associated variables themselves, suggesting a biexponential model is not appropriate for these actively passivated data.

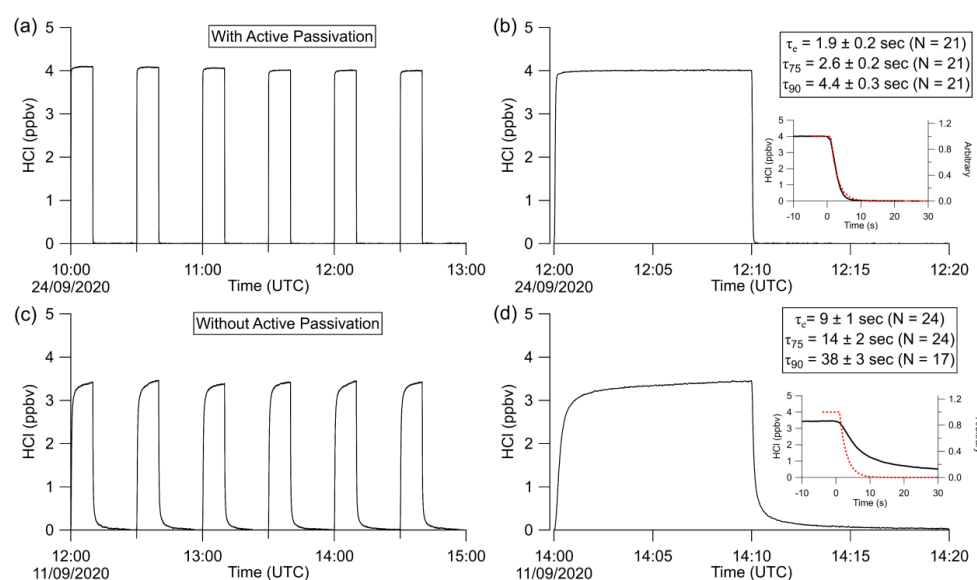


**Figure 5:** Excerpted time series of HCl permeation source additions with (a, b) and without (c, d) use of active passivation. a) TILDAS response to HCl permeation source addition to the sample line for 10 minutes every 30 minutes. b) Example case from plot (a) demonstrating the profile of the decay timescales. Reported  $\tau$ 's represents the mean and standard deviation of the entirety of these experiments. Inset shows a close-up of the actual decay compared with the red dashed line, representing the theoretical decay profile of a non-sticky compound modelled on the residence time of air in the absorption cell. Frames c) and d) are analogous to a) and b), but without use of active passivation.

Without active passivation, the signal profiles of the HCl additions have comparatively slower rises, and do not reach the average HCl maximum mixing ratios of  $4.03 \pm 0.06$  ppbv within 10 min intervals (Fig. 5a, b, Fig. A2). In these cases, biexponential models were fit without having to adjust the default convergence tolerance, and the results were found to have smaller term- and residual errors when compared to the analogous single exponential model (see Table A2).  $\tau_e$  for the signal decays was calculated as  $9 \pm 1$  s (N = 24), or approximately 4.5 times greater than the residence time through the measurement cell (Fig. 5c, d).

The reported timescales in this work can be further improved by increasing the flow rate of the inlet. Using the 12.7 slpm inertial inlet,  $\tau_e$  averaged  $0.49 \pm 0.03$  s (N=21), comparing very well to the theoretical cell residence time ( $1/e$ ) of 0.45 s for this flow rate (Fig. 6, Fig. A3, Table A3).  $\tau_{90}$  was similarly improved, averaging  $1.15 \pm 0.06$  s. The higher flow rate clearly demonstrates that wall interactions are reduced; as demonstrated by Fig. 6, the decay rate mimics that of methane, which is a non-sticky compound also measured by the HCl-TILDAS. As the current configuration includes 3 m of heated tubing between the inertial inlet and the HCl-TILDAS itself, it is likely this response could be further improved by shortening this line.

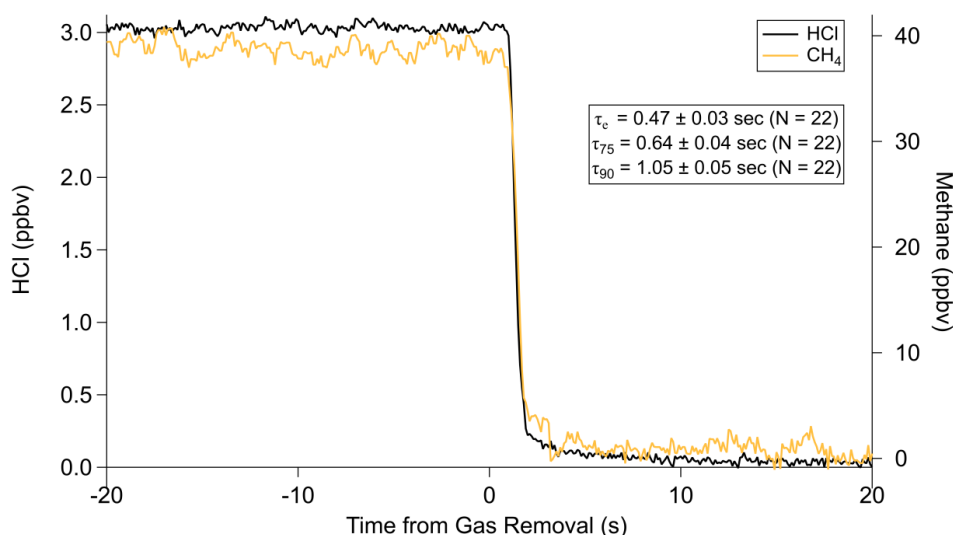
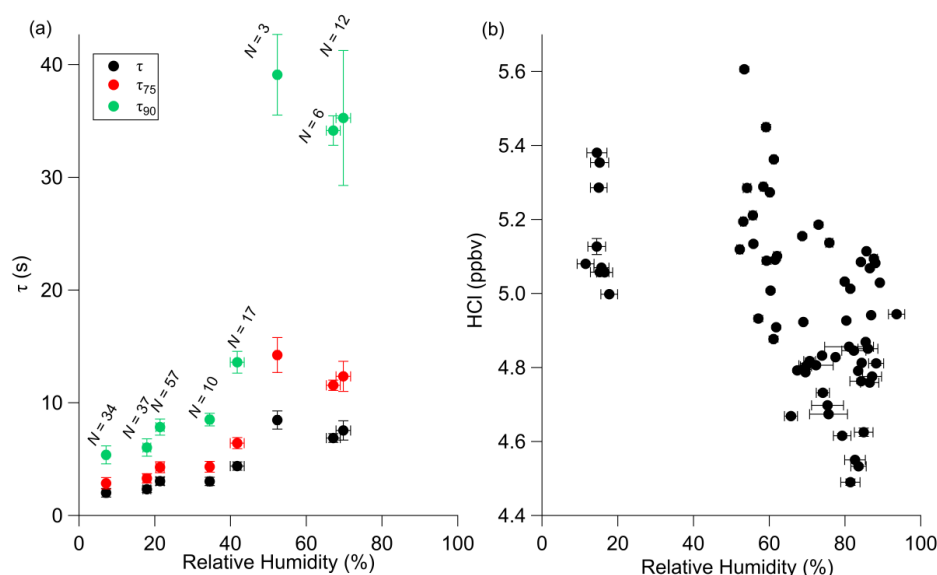


Figure 6: Comparison of HCl decay with methane at inlet flow rate of 12.7 slpm.

The  $\tau_{90}$  achieved utilizing active passivation in this study is the shortest reported instrument response time for changes in HCl mixing ratios to date (Table 1) and demonstrates that the use of PFBS is effective for reducing HCl-surface interactions. Previous studies have suggested that a biexponential model (Eq. 1) may better physically represent sticky gas flow through an instrument (Furlani et al., 2021; Zahniser et al., 1995; Ellis et al., 2010; Pollack et al., 2019); in this approach,  $\tau_1$  may represent the air residence time within the instrument, while  $\tau_2$  will represent the factor(s) that cause the analyte to lag through the instrument (e.g., surface interactions). Our results were not inconsistent with this postulation since the unpassivated cases were well-represented by the biexponential model (i.e., significant  $\tau_1$  and  $\tau_2$  equation terms within Eq. 1), while passivated cases were better represented by the single exponential model (i.e., dominant  $\tau_1$  but negligible  $\tau_2$ ). However, the results do not directly support it either; for unpassivated cases, the predicted  $\tau_1$  averaged  $6.2 \pm 0.7$  (greater than 3 times the cell residence time for the inertial inlet used), and  $69 \pm 10$  for  $\tau_2$  (Table A2). Further reconciliation of the physical basis behind the biexponential model is outside the scope of this work, and no attempt is made to ascribe further physical meaning to the derived coefficients.

### 3.2.2 Humidity

The experiments in the previous sections were conducted using dried compressed air. As dry air is not representative of ambient sampling conditions, timescale experiments were also performed with humidified sample air under passivated conditions. The results in Fig. 7a demonstrate a clear increase in  $\tau$ 's with increasing relative humidity, affecting  $\tau_{90}$  most prominently.



**Figure 7: Effects of changes in relative humidity on a)  $\tau$  in laboratory experiments and b) HCl standard mixing ratios in the field. Relative humidity values are based on the TILDAS-observed water mixing ratio observed during the HCl decay period (a) or HCl standard addition (b), and concurrent temperature reading. Error bars for both axes represent one standard deviation.**

While Roscioli et al. (2016) note that the general effectiveness of active passivation on  $\text{HNO}_3$  instrument response times appeared independent of humidity levels between 0–70%, the results of this experiment do not display this same behavior above approximately 40% relative humidity. Notably, the inlet flow rate used for these experiments is less than four times that used in that study (i.e.,  $2.8 \text{ L min}^{-1}$  vs  $14 \text{ L min}^{-1}$ ), which would increase analyte-surface interactions. However, these values do represent an improvement from the HCl sampling method reported by Furlani et al. (2021), in which  $\tau_{90}$  was reported as 239s at 33% relative humidity. Similarly, field additions of a HCl permeation source (utilizing the  $3.7 \text{ L min}^{-1}$  inertial inlet) elicited lower mixing ratios at relative humidities above 60% (mean of  $4.9 \pm 0.2$  ppbv), contrasting with additions under dry air conditions (i.e., relative humidities below 20%; mean of  $5.2 \pm 0.1$  ppbv) (Fig. 7b). This finding suggests that a permanent or semi-permanent physical loss of HCl is occurring within the sampling inlet at higher humidities, resulting in an average -5.8% bias. Both PFA tubing and silica surfaces have been previously reported to adsorb several monolayers-worth of water at room temperature in humid air (Saliba et al., 2001; Sumner et al., 2004), which would be expected to bind and solvate HCl. As both the inertial inlet and sample line were heated to  $50^\circ\text{C}$ , it is anticipated that this effect would be minimised by discouraging water from attaching to surfaces, but not eliminated. However, increasing the sampling temperatures may further improve both the instrument response timescale and reduce this loss effect; warmer temperatures may also increase the likelihood of HCl degassing from coarse mode particles within the inertial inlet before their removal, or from fine mode particles that may travel throughout the entire sample path (Brimblecombe and Clegg, 1988). Further discussion of the effects of particulate chloride and uncertainty estimation can be found in Sect. 3.3.1.





### 396 3.3 Potential Interferences

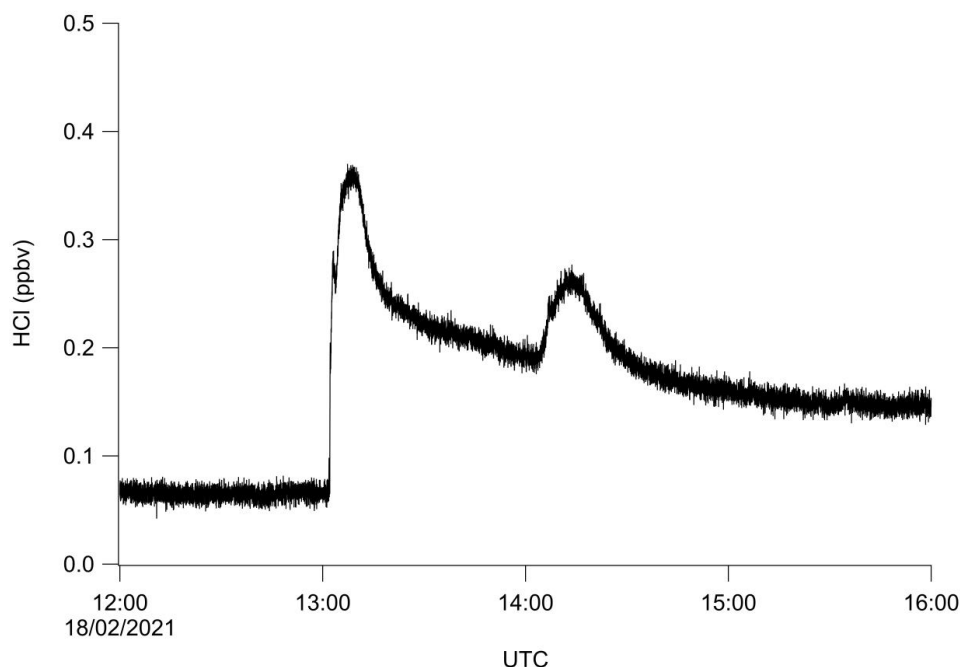
397 As discussed above, spectral interferences are not believed to play a major role in the detected HCl concentrations.  
 398 However, two potential sources of undesired HCl may exist if sample gas contains a significant amount of  
 399 particulate chloride ( $\text{pCl}^-$ ) or other strong gaseous acids (e.g.,  $\text{HNO}_3$ ), discussed in more detail below.

#### 400 3.3.1 Effects of Particulate Chloride

401 It is well established that HCl and particulate chloride ( $\text{pCl}^-$ ) exist together in dynamic equilibrium. The use of  
 402 heated sample inlet lines (50 °C in this study) may volatilize HCl from  $\text{pCl}^-$  if sufficient heating occurs before  
 403 particles are removed via impaction, yielding measurements with positive systematic error. As discussed in Sect.  
 404 2.6.3, the thermodynamic equilibrium model ISORROPIA II was used to theoretically assess the impact of  $\text{pCl}^-$   
 405 volatilisation within the heated TILDAS sample inlet on measured HCl mixing ratios based on three potential  
 406 operating temperatures (35°C, 50°C, and 80°C). To simulate conditions of an inland, urban environment, averaged  
 407 aerosol concentrations from London, England, were used to initiate the model (Crilley et al., 2017; Bandy et al.,  
 408 2022b, a). It was estimated for the conditions of these measurements that HCl repartitioning from  $\text{pCl}^-$  would  
 409 result in an increase of the HCl mixing ratio by 1 ppqv at both 35°C and 50 °C, while dramatically increasing to  
 410 200 pptv at 80°C. Such increases in HCl are expected to derive from the loss of the liquid aerosol phase following  
 411 the reduction in humidity experienced in the elevated temperatures of the sample inlet, and the evaporation of  
 412  $\text{NH}_4\text{Cl}$ . However, Huffman et al. (2009) reported approximately the evaporation of only 10-15%  $\text{NH}_4\text{Cl}$  aerosol  
 413 through a thermodenuder held at 50 °C (12 s residence time). Based on an inertial inlet flow rate of  $2.8 \text{ L min}^{-1}$   
 414 and a corresponding residence time of 150 ms before particulate removal via impaction, it is unlikely volatilization  
 415 will significantly affect these measurements. Further in situ testing was performed during the OSCA field study,  
 416 discussed further in Sect. 3.4.

#### 417 3.3.2 Effects of Nitric Acid

418 The use of PFBS appears to lessen the effects of HCl surface adsorption and improve the instrument response  
 419 time to changes in HCl concentrations (Fig. 5, 6). If, though, PFBS does not completely prevent HCl sorbing to  
 420 walls, the sampling of acids stronger than HCl (e.g.,  $\text{HNO}_3$ ) may perturb the existing passivation equilibrium on  
 421 instrument surfaces. In order to test this, a  $\text{HNO}_3$  permeation source was fabricated (Sect. 2.4) and allowed to  
 422 flow into the TILDAS inlet (Fig. 8). The  $\text{HNO}_3$  permeation source output was estimated as NO using a Mo-  
 423 catalyzed  $\text{NO}_y$  convertor in tandem with a commercial  $\text{NO}_x$  analyzer (Teledyne T200). In a test experiment, the  
 424 addition of 4.0 ppbv of  $\text{HNO}_3$  to the inertial inlet caused a maximum increase of 0.29 ppbv to the HCl signal (Fig.  
 425 8). Continued addition of  $\text{HNO}_3$  eventually causes the signal to plateau at a higher background, ~0.08 ppbv above  
 426 the original background.



427 **Figure 8: Demonstration of the effects of 4.0 ppbv nitric acid addition to the passivated sample inlet flow at**  
 428 **approximately 13:00 UTC.**

429 There is no absorption band overlap between  $\text{HNO}_3$  and  $\text{HCl}$  in the analyzed spectral region, strongly  
 430 indicating the observed increase in  $\text{HCl}$  signal occurred due to additional  $\text{HCl}$  molecules reaching the absorption  
 431 cell. It is plausible this occurs because of interactions between  $\text{HNO}_3$  and surfaces where  $\text{HCl}$  may be adsorbed,  
 432 or with sampled particulates. One possible mechanism is that the  $\text{HNO}_3$  increases competition for sorption sites,  
 433 and ultimately replaces  $\text{HCl}$  on the surface. In this scenario, expected behavior would be a gradual increase in the  
 434 background  $\text{HCl}$  signal as the stronger acid removes available sorption sites, and increased  $\text{HCl}$  throughput is  
 435 achieved. A second mechanism would occur if water or particulate  $\text{Cl}^-$  are present on instrument surfaces; here,  
 436 the diffusion of the  $\text{HNO}_3$  into the water would cause acid displacement of  $\text{HCl}$ , as in Reaction (R2). If the strong  
 437 acid flux were large enough, a sharp  $\text{HCl}$  signal increase (commensurate with the magnitude of available  $\text{Cl}^-$ )  
 438 would be anticipated from  $\text{HCl}$  off-gassing that would gradually recover as a new equilibrium is established. As  
 439 seen in Fig. 8, it appears that a combination of these mechanisms is present. Once equilibrium had been  
 440 established with addition of  $\text{HNO}_3$ , flow from additional  $\text{HNO}_3$  permeation sources were added to the inertial inlet  
 441 to observe whether additional  $\text{HCl}$  would be driven off (results not shown). However, each addition of  $\text{HNO}_3$   
 442 resulted in similar spikes and signal recoveries to elevated  $\text{HCl}$  background levels. As the sudden introduction of  
 443 4.0 ppbv  $\text{HNO}_3$  into the TILDAS inlet produced  $< 10\%$  of a signal response, it is likely a more gradual introduction  
 444 of  $\text{HNO}_3$  would elicit a proportionally smaller  $\text{HCl}$  signal. Further, Fig. 8 was produced using an inertial inlet  
 445 flow rate of  $2.8 \text{ L min}^{-1}$ ; these mechanisms are expected to be further reduced using faster-flow inlets (e.g.,  $12.7$   
 446  $\text{L min}^{-1}$ ), which would both reduce gas-surface interactions, as well as make the mixing ratio transient  
 447 proportionally smaller.

While this interference was shown to be of potential significance in a laboratory context, in situ effects cannot be quantified without concurrent  $\text{HNO}_3$  (or proxy) observations. To this end, estimations of how  $\text{HNO}_3$  affects our method in a real-world context are further explored in Sect. 3.4.

### 3.4 Field Sampling

Field observations for HCl-TILDAS were obtained during the Summer 2021 OSCA campaign, hosted at the University of Manchester (Sect. 2.4; Fig. 9). These represent the second high frequency tropospheric field measurement of HCl reported by optical techniques (Angelucci et al., 2021). For the period presented, ambient relative humidity ranged from 36–98%, and corresponded with average  $\tau_e$  of  $2.8 \pm 0.3$  s ( $\tau_{90} = 7 \pm 1$  s). Because the inertial inlet used in this study had a flow rate of  $3.7 \text{ L min}^{-1}$ , the expected  $1/e$  residence time in the Herriott cell is approximately 1.5 s; these longer empirical instrument response timescales indicate incomplete passivation of inlet surfaces. Further, as discussed in Sect. 3.2.2, it is expected that the magnitude of the HCl measurements will be biased low by as much as 5.8% in this campaign due to inlet surface losses, quantified through regular field additions of a HCl permeation standard (Fig. 7).

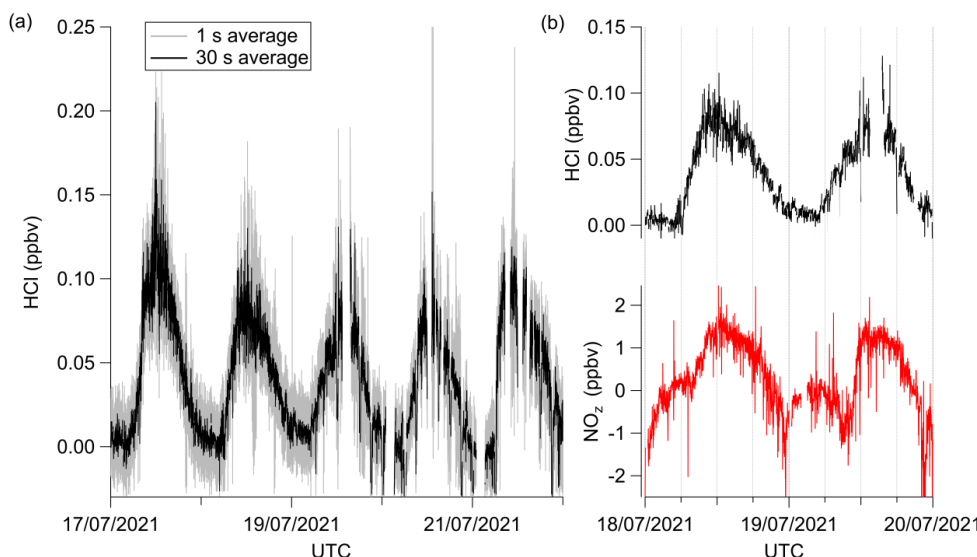


**Figure 9** – Excerpted field data from summer OSCA 2021 campaign. a) Averaged time series during the final week of measurements, in which grey represents 1 s data collection frequency, while the black trace represents 30 s averages of these same data. b) Comparison of HCl time series (top) and concurrent  $\text{NO}_x$  time series, both averaged to 1 min.

Additional sources of uncertainty may be introduced from plumes of  $\text{HNO}_3$  sampled by our inlet, as discussed in Sect. 3.3.2. While no direct  $\text{HNO}_3$  measurement was obtained during the OSCA campaign,  $\text{NO}_x$  was used as an approximation, calculated from co-located  $\text{NO}_x$  and  $\text{NO}_y$  observations ( $\text{NO}_x = \text{NO}_y - \text{NO} - \text{NO}_2$ ) (Watson, 2022c, b). For the period presented in Fig. 9b, a Pearson correlation coefficient ( $r$ ) of 0.69 was found between HCl and  $\text{NO}_x$ . Given both compounds ambient production pathways are expected to follow a photochemically driven diurnal cycle, this suggestion of linearity is not surprising. However, the profiles themselves differ, with changes in  $\text{NO}_x$  lagging changes in HCl. For example, HCl mixing ratios begin to rise at 06:00 on 18 July 2021, while  $\text{NO}_x$  mixing ratios remain comparatively plateaued until 08:00, when it begins its



472 rise. A similar pattern repeats on 19 July 2021, in which HCl mixing ratios begin rising just before 06:00, and  
473 NO<sub>x</sub> mixing ratios again do not increase until 08:00. The sharp increase in NO<sub>x</sub> mixing ratios after 08:00 is not  
474 followed by an in-kind increase in HCl mixing ratios; if HNO<sub>3</sub> were eliciting HCl within the sample inlet, it would  
475 be expected fluxes of HNO<sub>3</sub> would precede or coincide with increases in HCl. As such, we do not believe HNO<sub>3</sub>  
476 is a significant interference within our inlet for the period analysed here.

477 To test the extent to which pCl<sup>-</sup> may repartition to HCl, a denuder was temporarily fitted in line to sample  
478 only pCl<sup>-</sup>; consequently, any HCl observed during the time period could be attributed to the re-partitioning of pCl<sup>-</sup>  
479 within the TILDAS sample inlet (Fig. 10). To confirm the efficacy of removing HCl gas, cylinder additions that  
480 result in TILDAS observed mixing ratios of 2.8, 35, and 69 ppbv were injected through the denuder for 60s with  
481 no corresponding increase in TILDAS signal (Fig. 10c). For the period presented, HCl signal was seen to range  
482 between limits of detection to peaking at 53 pptv. ISORROPIA was used to test how much HCl may originate  
483 from pCl<sup>-</sup> in the conditions during the OSCA campaign, utilizing co-located measurements of total (gas + aerosol)  
484 concentrations of NH<sub>3</sub> and HNO<sub>3</sub> (as NO<sub>x</sub>) (Watson, 2022c, b, a) within the heated inlet system using the ‘forward’  
485 mode in ISORROPIA (no metals were included in these calculations). Based on these simulations, it was expected  
486 that the majority of pCl<sup>-</sup> would partition into the gas phase upon reaching thermal equilibrium in the sample inlet  
487 leading to systematic errors of up to 40, 43, and 48 pptv at 308, 323, and 353 K respectively. While the HCl signal  
488 did reach these values while the denuder was installed, no direct relationship was observed between the HCl signal  
489 and concurrent pCl<sup>-</sup> measurements (Fig. 10a, b). In particular, there are instances (e.g., between 12:00-15:00 on  
490 20 June 2022) where the available chlorine (calculated as the mixing ratio of chlorine if it were entirely released  
491 from particulates) is less than HCl observations. This may suggest a potential leak between the denuder and the  
492 inertial inlet that could allow a small volume of ambient air to contaminate the air sample, obfuscating accurate  
493 interpretation of these results. While a strong relationship was not observed between the pCl<sup>-</sup> and HCl signals  
494 (with denuder) in the period observed here, the ISOROPPIA predictions emphasize that this is a significant  
495 possible source of positive error in HCl measurements whenever heated sample lines are used for HCl sampling  
496 in the presence of particulates.

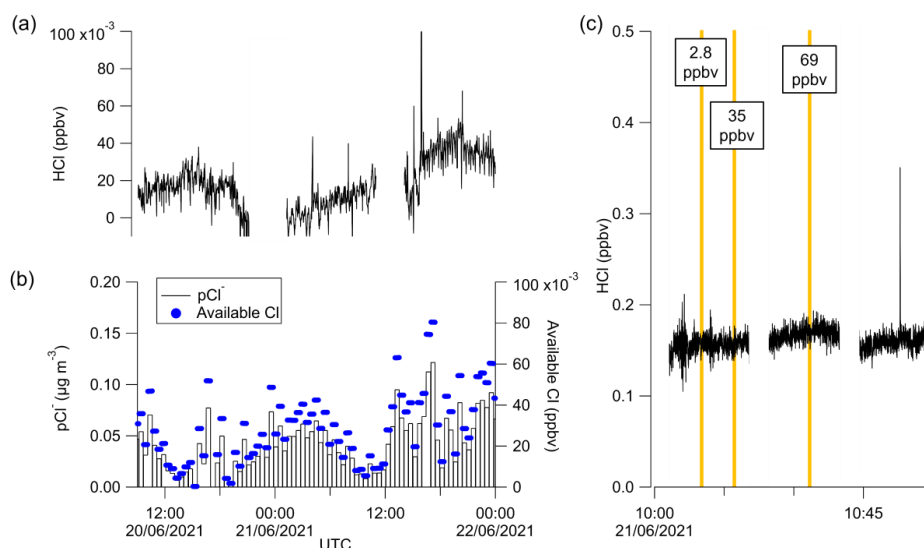


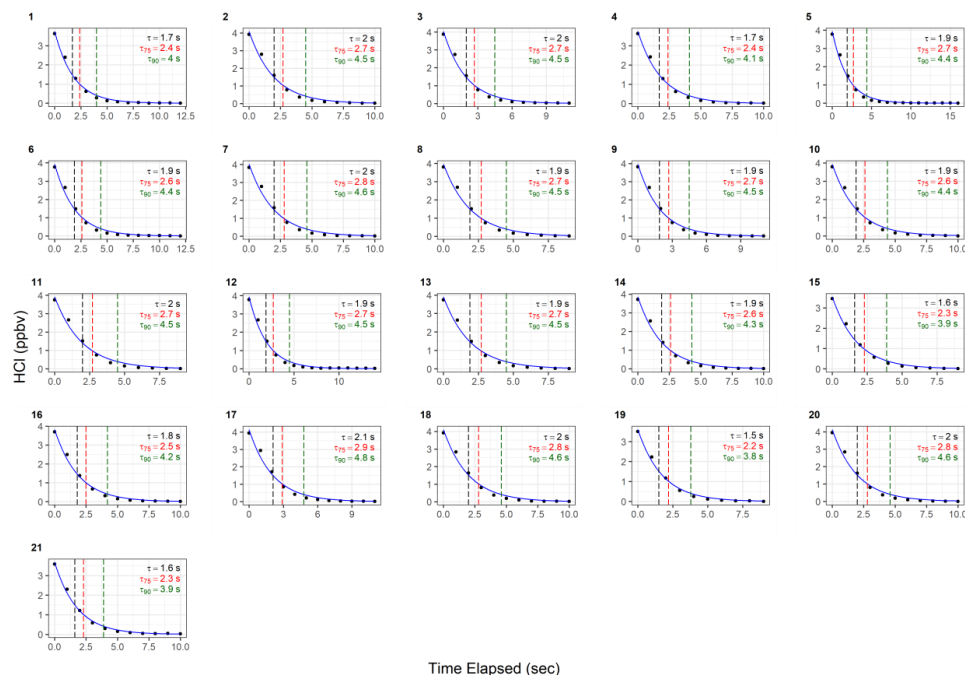
Figure 10: Time series of a) HCl when denuder was installed on HCl TILDAS inlet in comparison with b) pCl<sup>-</sup> observations. Available Cl was calculated by converting the pCl<sup>-</sup> concentrations into mixing ratios. c) HCl cylinder additions were conducted (yellow shading) to verify the denuder was removing gas phase HCl. The data in panel c) has neither been background corrected or time averaged.

#### 4 Conclusions

This work has demonstrated the viability of HCl-TILDAS for obtaining high-frequency observations of ambient HCl. The associated sampling method, involving a virtual impactor to avoid excess surface-mediated interactions with filters, as well as heat and chemical passivation to increase HCl throughput, was also shown to greatly improve instrument response to changes in HCl concentration. However, there is room for further innovation in obviating the stickiness of HCl, including additional heating of sampling lines, minimizing pressure within the sampling line, as well as utilizing higher flow inlets. The use of shorter inlets operating at higher flow rates will additionally reduce sample air residence time in the inlet, both reducing HCl-wall interactions and mitigating the likelihood of HCl partitioning out of particulates within the inlet. The fast time responses to changes in HCl mixing ratios shown herein will be well-suited for mobile sampling platforms, such as aircraft or vehicle-based laboratories, in which high temporal and spatial concentration variability are inherent. Finally, the potential for interferences from particulate chloride necessitates careful consideration for the method of obtaining background measurements. Regular installations of a denuder, or incorporation of a denuder into a background mechanism would minimize the uncertainty presented.

## 515 Appendix A

### Passivated HCl Decays (Dry)



516 **Figure A1 – Instrument response times to changes in HCl mixing ratios utilising active passivation. Black dots**  
 517 **represent observed data and are overlayed by the calculated single exponential model (according to the terms listed in**  
 518 **Table A1). Vertical hashed lines are placed on time elapsed corresponding to  $\tau_c$  (black),  $\tau_{75}$  (red), and  $\tau_{90}$  (green).**



Table A1 – Results for each model fit for determining the instrument response times under actively passivated conditions with the 2.8 L min<sup>-1</sup> inertial inlet, and corresponds with Fig. A1. Model parameters correspond to Eq. 1 in Sect. 2.6.2.

Single Exponential Fit							Bi-Exponential Fit							
Trial	$\tau_c$ (s)	$\tau_{75}$ (s)	$\tau_{90}$ (s)	$A_1$	$k_1$	Residuals	$\tau_c$ (s)	$\tau_{75}$ (s)	$\tau_{90}$ (s)	$A_1$	$k_1$	$A_2$	$k_2$	Residuals
1	1.7	2.4	4	$3.7 \pm 0.1$	$0.58 \pm 0.01$	0.10	1.4	2.1	4	$3.4 \pm 1.2$	$0.8 \pm 0.3$	$0.5 \pm 1.2$	$0.2 \pm 0.3$	0.20
2	2	2.7	4.5	$4.1 \pm 0.1$	$0.60 \pm 0.02$	0.16	1.9	2.8	4.9	$1.8 \pm 10.4$	$0.8 \pm 1.9$	$2.3 \pm 10.4$	$0.4 \pm 0.6$	0.22
3	2	2.7	4.5	$4.0 \pm 0.1$	$0.60 \pm 0.02$	0.14	1.8	2.6	4.9	$2.7 \pm 4.1$	$0.8 \pm 0.7$	$1.4 \pm 4.1$	$0.3 \pm 0.4$	0.23
4	1.7	2.4	4.1	$3.7 \pm 0.1$	$0.58 \pm 0.02$	0.11	1.7	2.4	4.2	$1.7 \pm 12.1$	$0.8 \pm 1.9$	$2.0 \pm 12.1$	$0.4 \pm 0.7$	0.16
5	1.9	2.7	4.4	$3.9 \pm 0.1$	$0.60 \pm 0.01$	0.11	1.9	2.8	5	$2.7 \pm 4.1$	$0.7 \pm 0.5$	$1.2 \pm 4.2$	$0.3 \pm 0.4$	0.17
6	1.9	2.6	4.4	$3.9 \pm 0.1$	$0.60 \pm 0.02$	0.13	1.9	2.7	4.9	$3.0 \pm 4.2$	$0.6 \pm 0.5$	$0.9 \pm 4.2$	$0.3 \pm 0.5$	0.20
7	2	2.8	4.6	$4.0 \pm 0.2$	$0.60 \pm 0.02$	0.17	1.9	2.8	4.9	$2.3 \pm 10.3$	$0.7 \pm 1.4$	$1.8 \pm 10.3$	$0.3 \pm 0.7$	0.24
8	1.9	2.7	4.5	$4.0 \pm 0.1$	$0.60 \pm 0.02$	0.16	2	2.8	4.7	$0.3 \pm 21.3$	$0.8 \pm 17.6$	$3.6 \pm 21.3$	$0.5 \pm 0.7$	0.19
9	1.9	2.7	4.5	$4.0 \pm 0.1$	$0.60 \pm 0.02$	0.14	1.9	2.7	4.8	$2.3 \pm 5.6$	$0.8 \pm 1.1$	$1.7 \pm 5.6$	$0.3 \pm 0.4$	0.21
10	1.9	2.6	4.4	$3.9 \pm 0.1$	$0.60 \pm 0.02$	0.14	2	2.7	4.2	$-4.5 \pm 40.0$	$1.0 \pm 1.6$	$8.3 \pm 40.0$	$0.7 \pm 0.5$	0.09
11	2	2.7	4.5	$3.9 \pm 0.2$	$0.60 \pm 0.02$	0.16	2	2.7	4.5	$4.9 \pm 40.5$	$0.6 \pm 0.9$	$-1.1 \pm 40.5$	$0.8 \pm 7.0$	0.16
12	1.9	2.7	4.5	$3.9 \pm 0.1$	$0.60 \pm 0.02$	0.12	1.6	2.2	4.2	$3.8 \pm 0.7$	$0.7 \pm 0.2$	$0.3 \pm 0.7$	$0.1 \pm 0.2$	0.26
13	1.9	2.7	4.5	$3.9 \pm 0.1$	$0.60 \pm 0.02$	0.16	2	2.8	4.6	$-1.2 \pm 54.2$	$0.8 \pm 7.6$	$5.0 \pm 54.2$	$0.5 \pm 1.1$	0.16
14	1.9	2.6	4.3	$3.9 \pm 0.1$	$0.59 \pm 0.02$	0.14	1.9	2.7	4.4	$-0.1 \pm 50.7$	$0.7 \pm 79.7$	$3.9 \pm 50.7$	$0.5 \pm 1.2$	0.15
15	1.6	2.3	3.9	$3.5 \pm 0.1$	$0.57 \pm 0.02$	0.10	1.6	2.3	4	$-0.5 \pm 48.7$	$0.8 \pm 15.5$	$4.0 \pm 48.7$	$0.6 \pm 1.1$	0.11
16	1.8	2.5	4.2	$3.8 \pm 0.1$	$0.59 \pm 0.02$	0.12	1.7	2.5	4.5	$1.9 \pm 8.7$	$0.8 \pm 1.6$	$2.0 \pm 8.8$	$0.4 \pm 0.6$	0.18
17	2.1	2.9	4.8	$4.1 \pm 0.2$	$0.62 \pm 0.02$	0.17	2.2	3	5	$0.5 \pm 23.4$	$0.8 \pm 11.1$	$3.6 \pm 23.4$	$0.4 \pm 0.7$	0.21
18	2	2.8	4.6	$4.1 \pm 0.2$	$0.61 \pm 0.02$	0.17	2	2.8	4.7	$1.4 \pm 39.6$	$0.4 \pm 2.6$	$2.7 \pm 39.5$	$0.6 \pm 2.5$	0.25
19	1.5	2.2	3.8	$3.6 \pm 0.1$	$0.56 \pm 0.02$	0.10	1.5	2.2	4	$0.9 \pm 9.3$	$0.9 \pm 4.0$	$2.7 \pm 9.3$	$0.5 \pm 0.5$	0.14
20	2	2.8	4.6	$4.1 \pm 0.2$	$0.60 \pm 0.02$	0.17								
21	1.6	2.3	3.9	$3.7 \pm 0.1$	$0.57 \pm 0.01$	0.09								



Unpassivated HCl Decays (Dry)

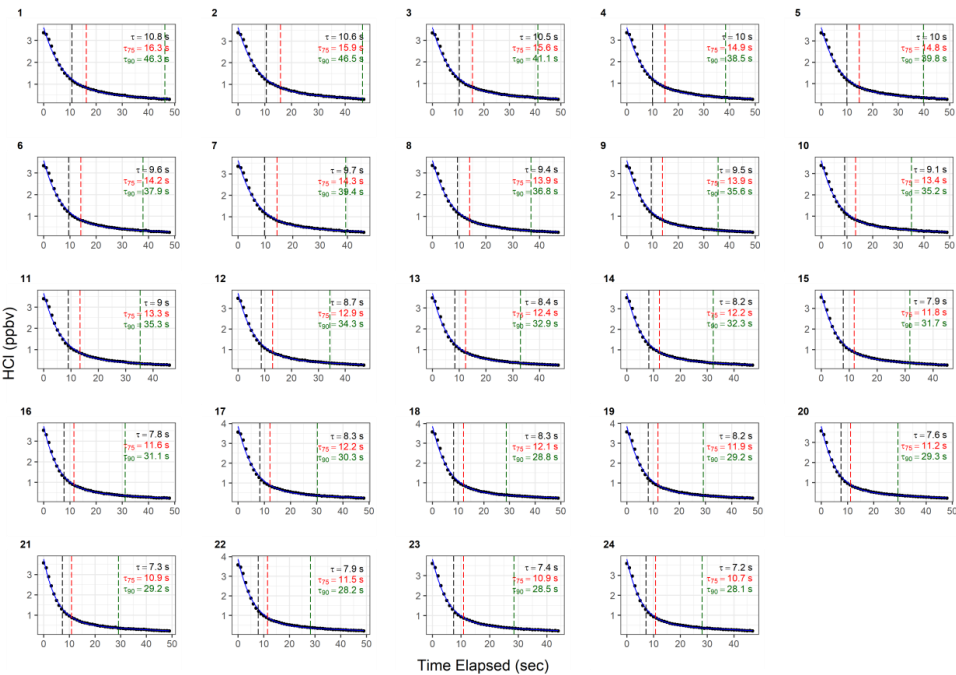


Figure A2 – Instrument response times to changes in HCl mixing ratios without active chemical passivation. Black dots represent observed data and are overlayed by the calculated bi-exponential model (according to the terms listed in Table A2). Vertical hashed lines are placed on time elapsed corresponding to  $\tau_c$  (black),  $\tau_{75}$  (red), and  $\tau_{90}$  (green).

529 **Table A2 – Results for each model fit for determining the instrument response times without use of active chemical**  
 530 **passivation, using the 2.8 L min<sup>-1</sup> inertial inlet, and corresponds with Fig. A2. Model parameters correspond to Eq. 1**  
 531 **in Sect. 2.6.2.**

Trial	Single Exponential Fit						Bi-Exponential Fit							
	$\tau_e$ (s)	$\tau_{75}$ (s)	$\tau_{90}$ (s)	$A_1$	$k_1$	Residuals	$\tau_e$ (s)	$\tau_{75}$ (s)	$\tau_{90}$ (s)	$A_1$	$k_1$	$A_2$	$k_2$	Residuals
1	13.7	19.4	33	$3.2 \pm 0.1$	$0.935 \pm 0.003$	0.21	11.3	17.5		$2.9 \pm 0.1$	$0.136 \pm 0.008$	$0.7 \pm 0.1$	$0.013 \pm 0.004$	0.06
2	13.5	19.1	32.4	$3.2 \pm 0.1$	$0.933 \pm 0.003$	0.21	11.1	17.1		$3.0 \pm 0.1$	$0.139 \pm 0.009$	$0.7 \pm 0.1$	$0.012 \pm 0.004$	0.06
3	13	18.3	30.8	$3.2 \pm 0.1$	$0.930 \pm 0.003$	0.20	10.8	16.4		$3.0 \pm 0.1$	$0.140 \pm 0.009$	$0.7 \pm 0.1$	$0.014 \pm 0.005$	0.06
4	12.7	17.9	30.3	$3.2 \pm 0.1$	$0.929 \pm 0.003$	0.20	10.5	16		$3.0 \pm 0.1$	$0.142 \pm 0.008$	$0.7 \pm 0.1$	$0.014 \pm 0.004$	0.06
5	12.6	17.8	30.1	$3.2 \pm 0.1$	$0.928 \pm 0.003$	0.21	10.4	15.8		$3.0 \pm 0.1$	$0.143 \pm 0.008$	$0.7 \pm 0.1$	$0.013 \pm 0.004$	0.06
6	12.4	17.6	29.8	$3.2 \pm 0.1$	$0.928 \pm 0.004$	0.22	10.1	15.5		$3.0 \pm 0.1$	$0.148 \pm 0.008$	$0.7 \pm 0.1$	$0.013 \pm 0.004$	0.06
7	11.9	16.7	28.1	$3.3 \pm 0.1$	$0.923 \pm 0.004$	0.20	10	14.9		$3.1 \pm 0.1$	$0.144 \pm 0.010$	$0.6 \pm 0.1$	$0.011 \pm 0.006$	0.07
8	11.4	16	27.1	$3.2 \pm 0.1$	$0.920 \pm 0.004$	0.19	9.6	14.3	42.2	$3.0 \pm 0.1$	$0.150 \pm 0.009$	$0.6 \pm 0.1$	$0.014 \pm 0.005$	0.06
9	11.6	16.2	27.3	$3.2 \pm 0.1$	$0.920 \pm 0.004$	0.20	9.7	14.5	43.1	$3.1 \pm 0.1$	$0.147 \pm 0.009$	$0.6 \pm 0.1$	$0.012 \pm 0.005$	0.07
10	11.3	16	27.1	$3.2 \pm 0.1$	$0.921 \pm 0.004$	0.21	9.4	14.1	43.1	$3.0 \pm 0.1$	$0.155 \pm 0.008$	$0.6 \pm 0.1$	$0.014 \pm 0.004$	0.06
11	11	15.5	26.1	$3.3 \pm 0.1$	$0.918 \pm 0.004$	0.21	9.2	13.8	42.1	$3.1 \pm 0.1$	$0.156 \pm 0.009$	$0.6 \pm 0.1$	$0.014 \pm 0.005$	0.06
12	10.7	15.1	25.5	$3.3 \pm 0.1$	$0.916 \pm 0.004$	0.21	8.9	13.4	39.4	$3.1 \pm 0.1$	$0.162 \pm 0.009$	$0.6 \pm 0.1$	$0.016 \pm 0.005$	0.06
13	10.5	14.9	25.3	$3.3 \pm 0.1$	$0.916 \pm 0.004$	0.22	8.6	13	39.7	$3.1 \pm 0.1$	$0.169 \pm 0.009$	$0.7 \pm 0.1$	$0.016 \pm 0.004$	0.06
14	10.3	14.6	24.9	$3.3 \pm 0.1$	$0.915 \pm 0.004$	0.22	8.4	12.8	38.9	$3.1 \pm 0.1$	$0.172 \pm 0.009$	$0.7 \pm 0.1$	$0.017 \pm 0.004$	0.06
15	9.9	14.1	24.1	$3.3 \pm 0.1$	$0.912 \pm 0.005$	0.22	8.1	12.3	37.8	$3.1 \pm 0.1$	$0.181 \pm 0.008$	$0.7 \pm 0.1$	$0.018 \pm 0.004$	0.05
16	9.9	14.2	24.3	$3.3 \pm 0.1$	$0.913 \pm 0.005$	0.22	8	12.2	37.6	$3.1 \pm 0.1$	$0.181 \pm 0.008$	$0.7 \pm 0.1$	$0.018 \pm 0.003$	0.05
17	10.2	14.3	24.1	$3.5 \pm 0.1$	$0.910 \pm 0.005$	0.22	8.6	12.7	36.9	$3.3 \pm 0.1$	$0.164 \pm 0.010$	$0.6 \pm 0.1$	$0.013 \pm 0.006$	0.08
18	10.1	14.2	23.9	$3.5 \pm 0.1$	$0.910 \pm 0.005$	0.22	8.5	12.6	35.4	$3.3 \pm 0.1$	$0.163 \pm 0.009$	$0.6 \pm 0.1$	$0.013 \pm 0.005$	0.07
19	10	14.1	23.7	$3.5 \pm 0.1$	$0.909 \pm 0.005$	0.22	8.4	12.4	35.8	$3.3 \pm 0.1$	$0.167 \pm 0.010$	$0.6 \pm 0.1$	$0.014 \pm 0.005$	0.07
20	9.6	13.6	23.1	$3.4 \pm 0.1$	$0.908 \pm 0.005$	0.23	7.8	11.7	36	$3.2 \pm 0.1$	$0.184 \pm 0.009$	$0.7 \pm 0.1$	$0.017 \pm 0.004$	0.06
21	9.3	13.4	23	$3.3 \pm 0.1$	$0.909 \pm 0.005$	0.23	7.5	11.4	35.4	$3.1 \pm 0.1$	$0.192 \pm 0.007$	$0.7 \pm 0.1$	$0.018 \pm 0.003$	0.05
22	9.7	13.7	23	$3.5 \pm 0.1$	$0.907 \pm 0.005$	0.23	8.1	12	34.4	$3.3 \pm 0.1$	$0.173 \pm 0.010$	$0.6 \pm 0.1$	$0.015 \pm 0.005$	0.08
23	9.2	13.1	22.2	$3.4 \pm 0.1$	$0.904 \pm 0.005$	0.22	7.6	11.4	34.2	$3.2 \pm 0.1$	$0.189 \pm 0.010$	$0.7 \pm 0.1$	$0.018 \pm 0.005$	0.06
24	9.1	13	22.1	$3.4 \pm 0.1$	$0.904 \pm 0.005$	0.23	7.4	11.2	34	$3.2 \pm 0.1$	$0.192 \pm 0.009$	$0.7 \pm 0.1$	$0.018 \pm 0.004$	0.06



Passivated HCl Decays (Dry)

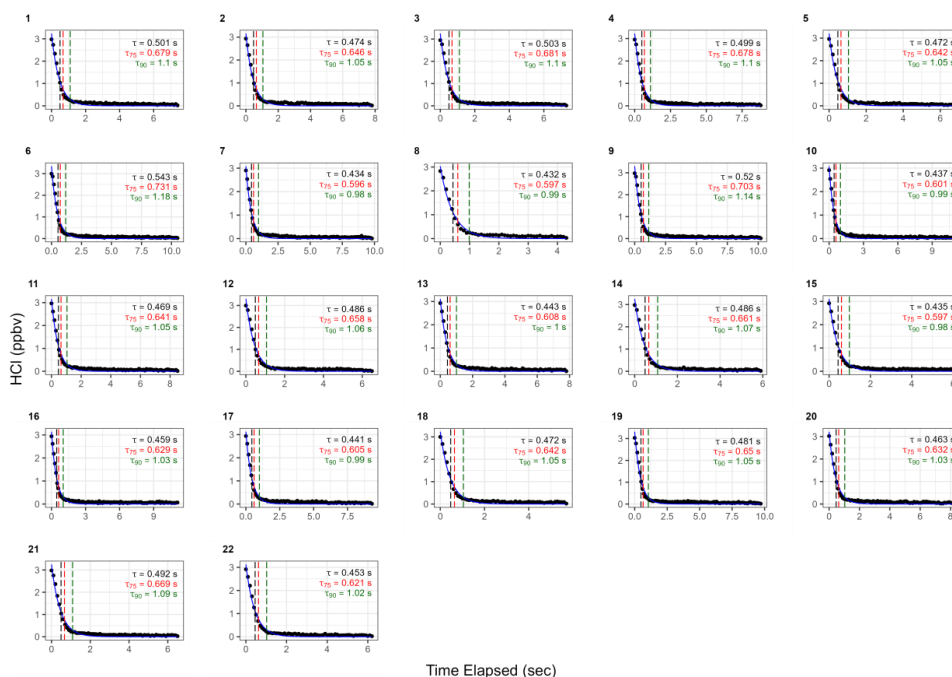


Figure A3: Instrument response times to changes in HCl mixing ratios with active chemical passivation and a high flow inertial inlet ( $12.7 \text{ L min}^{-1}$ ). Black dots represent observed data and are overlayed by the calculated single exponential model (according to the terms listed in Table A3). Vertical hashed lines are placed on time elapsed corresponding to  $\tau_c$  (black),  $\tau_{75}$  (red), and  $\tau_{90}$  (green).



537 **Table A3: Results for each model fit for determining the instrument response times under actively passivated conditions**  
 538 **with the 12.7 L min<sup>-1</sup> inertial inlet. Model parameters correspond to Eq. 1 in Sect. 2.6.2.**

Trial	Single Exponential Fit					Residuals
	$\tau_e$ (s)	$\tau_{75}$ (s)	$\tau_{90}$ (s)	$A_1$	$k_1$	
1	0.50	0.68	1.10	$3.24 \pm 0.08$	$0.113 \pm 0.009$	0.10
2	0.47	0.65	1.06	$3.16 \pm 0.08$	$0.106 \pm 0.009$	0.10
3	0.50	0.68	1.11	$3.25 \pm 0.08$	$0.12 \pm 0.01$	0.10
4	0.50	0.68	1.10	$3.22 \pm 0.07$	$0.115 \pm 0.009$	0.09
5	0.47	0.64	1.05	$3.21 \pm 0.08$	$0.103 \pm 0.009$	0.10
6	0.54	0.73	1.18	$3.34 \pm 0.07$	$0.129 \pm 0.009$	0.10
7	0.43	0.60	0.98	$3.08 \pm 0.06$	$0.093 \pm 0.007$	0.08
8	0.43	0.60	0.99	$3.03 \pm 0.08$	$0.10 \pm 0.01$	0.11
9	0.52	0.70	1.14	$3.30 \pm 0.07$	$0.121 \pm 0.009$	0.10
10	0.44	0.60	0.99	$3.08 \pm 0.06$	$0.095 \pm 0.007$	0.08
11	0.47	0.64	1.05	$3.16 \pm 0.07$	$0.106 \pm 0.008$	0.09
12	0.49	0.66	1.07	$3.30 \pm 0.08$	$0.105 \pm 0.009$	0.11
13	0.44	0.61	1.00	$3.11 \pm 0.07$	$0.097 \pm 0.008$	0.09
14	0.49	0.66	1.08	$3.25 \pm 0.08$	$0.109 \pm 0.009$	0.10
15	0.44	0.60	0.98	$3.10 \pm 0.08$	$0.092 \pm 0.008$	0.10
16	0.46	0.63	1.03	$3.14 \pm 0.06$	$0.103 \pm 0.007$	0.08
17	0.44	0.61	0.99	$3.13 \pm 0.07$	$0.095 \pm 0.008$	0.09
18	0.47	0.64	1.05	$3.23 \pm 0.08$	$0.104 \pm 0.009$	0.10
19	0.48	0.65	1.05	$3.32 \pm 0.07$	$0.102 \pm 0.008$	0.09
20	0.46	0.63	1.03	$3.21 \pm 0.07$	$0.101 \pm 0.008$	0.09
21	0.49	0.67	1.09	$3.25 \pm 0.07$	$0.112 \pm 0.009$	0.10
22	0.45	0.62	1.02	$3.13 \pm 0.07$	$0.101 \pm 0.008$	0.09

## 539 Acknowledgements

540 This program of work was primarily supported by the European Research Council (ERC-StG 802685). The  
 541 Aerodyne Research Inc. HCl instrument development work was funded by the NOAA Small Business Innovation  
 542 Research Program (WC-133R-17-CN-0092), and the Manchester field measurements were supported by the  
 543 NERC SPF OSCA project (NE/T001917/1). The authors would also like to thank Abigail Mortimer, Stuart  
 544 Murray, Chris Rhodes, and Mark Roper in the University of York Chemistry workshops, as well as Christopher  
 545 Anthony, for technical support, and Stuart Lacy in the University of York Wolfson Atmospheric Chemistry  
 546 Laboratory for data analysis software support. Further, the authors thank Michael Agnese and Michael Moore for  
 547 TILDAS technical support. The authors would like to acknowledge the efforts Conner Daube made in testing  
 548 configuration and sampling procedures on the companion HCl instrument. The author would also like to  
 549 acknowledge the spectroscopic analysis performed by J. Barry McManus to diagnose non-ideal noise sources and  
 550 design alignment optimizations. In addition, the authors thank James Lee, Will Drysdale, and Katie Read for their  
 551 support in laboratory experiments involving HNO<sub>3</sub> quantification.



552 **Code availability**

553 The code used to perform the calculations used in this study will be made publicly available on completion of the  
554 review process. In the meantime, data can be obtained upon request from the corresponding author.

555 **Data availability**

556 The data used in this study will be made publicly available on completion of the review process. In the meantime,  
557 data can be obtained upon request from the corresponding author.

558 **Author contribution**

559 SCH, JRR, CD, and TIY designed, built, and tested the HCl TILDAS at Aerodyne Research, Inc. SSB and PRV  
560 were involved in the initial HCl detector testing and support of Aerodyne Research, Inc., instrument development.  
561 JWH and PME designed laboratory and field experiments, and JWH conducted laboratory and field experiments.  
562 SJA designed and constructed bespoke temperature controlling units for the inertial inlet, the field inlet box, and  
563 permeation source ovens. JS performed ISOROPPIA modelling experiments. MF provided NO<sub>x</sub> and NO<sub>y</sub> data,  
564 as well as provided critical field support during the OSCA campaign. JWH prepared the manuscript, and all  
565 authors reviewed the manuscript.

566 **Competing interests**

567 The authors declare that they have no conflict of interest.

568 **References**

- 569 Abbatt, J., Oldridge, N., Symington, A., Chukalovskiy, V., McWhinney, R. D., Sjostedt, S., and Cox, R. A.:  
570 Release of Gas-Phase Halogens by Photolytic Generation of OH in Frozen Halide–Nitrate Solutions: An Active  
571 Halogen Formation Mechanism?, *J. Phys. Chem. A*, 114, 6527–6533, <https://doi.org/10.1021/jp102072t>, 2010.
- 572 Allan, W., Lowe, D. C., and Cainey, J. M.: Active chlorine in the remote marine boundary layer: Modeling  
573 anomalous measurements of  $\delta^{13}\text{C}$  in methane, *Geophys. Res. Lett.*, 28, 3239–3242,  
574 <https://doi.org/10.1029/2001GL013064>, 2001.
- 575 Angelucci, A. A., Furlani, T. C., Wang, X., Jacob, D. J., VandenBoer, T. C., and Young, C. J.: Understanding  
576 Sources of Atmospheric Hydrogen Chloride in Coastal Spring and Continental Winter, *ACS Earth Space Chem.*,  
577 5, 2507–2516, <https://doi.org/10.1021/acsearthspacechem.1c00193>, 2021.
- 578 Atkinson, R., Baulch, D. L., Cox, R. A., Crowley, J. N., Hampson, R. F., Hynes, R. G., Jenkin, M. E., Rossi, M.  
579 J., Troe, J., and IUPAC Subcommittee: Evaluated kinetic and photochemical data for atmospheric chemistry:  
580 Volume II - gas phase reactions of organic species, *Atmospheric Chem. Phys.*, 6, 3625–4055,  
581 <https://doi.org/10.5194/acp-6-3625-2006>, 2006.
- 582 Atkinson, R., Baulch, D. L., Cox, R. A., Crowley, J. N., Hampson, R. F., Hynes, R. G., Jenkin, M. E., Rossi, M.  
583 J., and Troe, J.: Evaluated kinetic and photochemical data for atmospheric chemistry: Volume III - gas phase





- 584 reactions of inorganic halogens, *Atmospheric Chem. Phys.*, 7, 981–1191, <https://doi.org/10.5194/acp-7-981-2007>,  
 585 2007.
- 586 Bandy, B., Faloon, K., Finessi, E., Lee, J. D., Leigh, R. J., Liu, D., Monks, P. S., Oram, D. E., Visser, S.,  
 587 Whitehead, J., and Young, D.: ClearfLo: IOP Summer Atmospheric Chemistry and meteorology measurements  
 588 and NAME Airmass Footprint dispersion model output at North Kensington, London, CAS Br. Atmospheric Data  
 589 Cent., <https://catalogue.ceda.ac.uk/uuid/4c35e63d6507408d96e4af3dce410e3d>, 2022a.
- 590 Bandy, B., Faloon, K., Finessi, E., Herndon, S. C., Laufs, S., Lee, J. D., Leigh, R. J., Liu, D., Monks, P. S., Oram,  
 591 D. E., Visser, S., Whitehead, J., Young, D., and Zotter, P.: ClearfLo: Longterm atmospheric chemistry and  
 592 meteorological measurements and NAME dispersion model output for ClearfLo, CAS Br. Atmospheric Data  
 593 Cent., <https://catalogue.ceda.ac.uk/uuid/f02d656eddf44f4283c085fc763a6f02>, 2022b.
- 594 Behnke, W. and Zetzsch, C.: Heterogeneous photochemical formation of Cl atoms from NaCl aerosol, NO<sub>x</sub> and  
 595 ozone, *J. Aerosol Sci.*, 21, S229–S232, [https://doi.org/10.1016/0021-8502\(90\)90226-N](https://doi.org/10.1016/0021-8502(90)90226-N), 1990.
- 596 Behnke, W., Krüger, H.-U., Scheer, V., and Zetzsch, C.: Formation of ClNO<sub>2</sub> and hono in the presence of NO<sub>2</sub>,  
 597 O<sub>3</sub> and wet NaCl aerosol, *J. Aerosol Sci.*, 23, 933–936, [https://doi.org/10.1016/0021-8502\(92\)90565-D](https://doi.org/10.1016/0021-8502(92)90565-D), 1992.
- 598 Behnke, W., George, C., Scheer, V., and Zetzsch, C.: Production and decay of ClNO<sub>2</sub> from the reaction of gaseous  
 599 N<sub>2</sub>O<sub>5</sub> with NaCl solution: Bulk and aerosol experiments, *J. Geophys. Res. Atmospheres*, 102, 3795–3804,  
 600 <https://doi.org/10.1029/96JD03057>, 1997.
- 601 Brimblecombe, P. and Clegg, S. L.: The solubility and behaviour of acid gases in the marine aerosol, *J.*  
 602 *Atmospheric Chem.*, 7, 1–18, <https://doi.org/10.1007/BF00048251>, 1988.
- 603 Buck, R. C., Franklin, J., Berger, U., Conder, J. M., Cousins, I. T., de Voogt, P., Jensen, A. A., Kannan, K.,  
 604 Mabury, S. A., and van Leeuwen, S. P.: Perfluoroalkyl and polyfluoroalkyl substances in the environment:  
 605 Terminology, classification, and origins, *Integr. Environ. Assess. Manag.*, 7, 513–541,  
 606 <https://doi.org/10.1002/ieam.258>, 2011.
- 607 Burkholder, J. B., Sander, S. P., Abbatt, J., Barker, J. R., Huie, R. E., Kolb, C. E., Kurylo, M. J., Orkin, V. L.,  
 608 Wilmouth, D. M., and Wine, P. H.: Chemical Kinetics and Photochemical Data for Use in Atmospheric Studies,  
 609 Evaluation No. 18, JPL Publication 15-10., Jet Propulsion Laboratory, Pasadena, 2015.
- 610 Clegg, S. L. and Brimblecombe, P.: The dissociation constant and henry’s law constant of HCl in aqueous solution,  
 611 *Atmospheric Environ.* 1967, 20, 2483–2485, [https://doi.org/10.1016/0004-6981\(86\)90079-X](https://doi.org/10.1016/0004-6981(86)90079-X), 1986.
- 612 Crilley, L. R., Lucarelli, F., Bloss, W. J., Harrison, R. M., Beddows, D. C., Calzolari, G., Nava, S., Valli, G.,  
 613 Bernardoni, V., and Vecchi, R.: Source apportionment of fine and coarse particles at a roadside and urban  
 614 background site in London during the 2012 summer ClearfLo campaign, *Environ. Pollut.*, 220, 766–778,  
 615 <https://doi.org/10.1016/j.envpol.2016.06.002>, 2017.
- 616 Crisp, T. A., Lerner, B. M., Williams, E. J., Quinn, P. K., Bates, T. S., and Bertram, T. H.: Observations of gas  
 617 phase hydrochloric acid in the polluted marine boundary layer, *J. Geophys. Res. Atmospheres*, 119, 6897–6915,  
 618 <https://doi.org/10.1002/2013JD020992>, 2014.
- 619 Eger, P. G., Helleis, F., Schuster, G., Phillips, G. J., Lelieveld, J., and Crowley, J. N.: Chemical ionization  
 620 quadrupole mass spectrometer with an electrical discharge ion source for atmospheric trace gas measurement,  
 621 *Atmospheric Meas. Tech.*, 12, 1935–1954, <https://doi.org/10.5194/amt-12-1935-2019>, 2019a.
- 622 Eger, P. G., Friedrich, N., Schuladen, J., Shenolikar, J., Fischer, H., Tadic, I., Harder, H., Martinez, M., Rohloff,  
 623 R., Tauer, S., Drewnick, F., Fachinger, F., Brooks, J., Darbyshire, E., Sciare, J., Pikridas, M., Lelieveld, J., and



- 624 Crowley, J. N.: Shipborne measurements of ClNO<sub>2</sub> in the Mediterranean Sea and around the Arabian Peninsula  
 625 during summer, *Atmospheric Chem. Phys.*, 19, 12121–12140, <https://doi.org/10.5194/acp-19-12121-2019>,  
 626 2019b.
- 627 Ellis, R. A., Murphy, J. G., Pattey, E., van Haarlem, R., O’Brien, J. M., and Herndon, S. C.: Characterizing a  
 628 Quantum Cascade Tunable Infrared Laser Differential Absorption Spectrometer (QC-TILDAS) for measurements  
 629 of atmospheric ammonia, *Atmospheric Meas. Tech.*, 3, 397–406, <https://doi.org/10.5194/amt-3-397-2010>, 2010.
- 630 Erickson, D. J., Seuzaret, C., Keene, W. C., and Gong, S. L.: A general circulation model based calculation of  
 631 HCl and ClNO<sub>2</sub> production from sea salt dechlorination: Reactive Chlorine Emissions Inventory, *J. Geophys. Res.*  
 632 *Atmospheres*, 104, 8347–8372, <https://doi.org/10.1029/98JD01384>, 1999.
- 633 Fickert, S., Adams, J. W., and Crowley, J. N.: Activation of Br<sub>2</sub> and BrCl via uptake of HOBr onto aqueous salt  
 634 solutions, *J. Geophys. Res. Atmospheres*, 104, 23719–23727, <https://doi.org/10.1029/1999JD900359>, 1999.
- 635 Fountoukis, C. and Nenes, A.: ISORROPIA II: a computationally efficient thermodynamic equilibrium model for  
 636 K<sup>+</sup>-Ca<sup>2+</sup>-Mg<sup>2+</sup>-NH<sub>4</sub><sup>+</sup>-Na<sup>+</sup>-SO<sub>4</sub><sup>2-</sup>-NO<sub>3</sub><sup>-</sup>-Cl-H<sub>2</sub>O aerosols, *Atmospheric Chem. Phys.*, 7, 4639–4659,  
 637 <https://doi.org/10.5194/acp-7-4639-2007>, 2007.
- 638 Frinak, E. K. and Abbatt, J. P. D.: Br<sub>2</sub> Production from the Heterogeneous Reaction of Gas-Phase OH with  
 639 Aqueous Salt Solutions: Impacts of Acidity, Halide Concentration, and Organic Surfactants, *J. Phys. Chem. A*,  
 640 110, 10456–10464, <https://doi.org/10.1021/jp063165o>, 2006.
- 641 Fu, X., Wang, T., Wang, S., Zhang, L., Cai, S., Xing, J., and Hao, J.: Anthropogenic Emissions of Hydrogen  
 642 Chloride and Fine Particulate Chloride in China, *Environ. Sci. Technol.*, 52, 1644–1654,  
 643 <https://doi.org/10.1021/acs.est.7b05030>, 2018.
- 644 Furlani, T. C., Veres, P. R., Dawe, K. E. R., Neuman, J. A., Brown, S. S., VandenBoer, T. C., and Young, C. J.:  
 645 Validation of a new cavity ring-down spectrometer for measuring tropospheric gaseous hydrogen chloride,  
 646 *Atmospheric Meas. Tech.*, 14, 5859–5871, <https://doi.org/10.5194/amt-14-5859-2021>, 2021.
- 647 von Glasow, R., Bobrowski, N., and Kern, C.: The effects of volcanic eruptions on atmospheric chemistry, *Chem.*  
 648 *Geol.*, 263, 131–142, <https://doi.org/10.1016/j.chemgeo.2008.08.020>, 2009.
- 649 Graedel, T. E. and Keene, W. C.: Tropospheric budget of reactive chlorine, *Glob. Biogeochem. Cycles*, 9, 47–77,  
 650 <https://doi.org/10.1029/94GB03103>, 1995.
- 651 Graedel, T. E. and Keene, W. C.: The Budget and Cycle of Earth’s Natural Chlorine, *Pure Appl. Chem.*, 68, 1689–  
 652 1697, <https://doi.org/10.1351/pac199668091689>, 1996.
- 653 Hagen, C. L., Lee, B. C., Franka, I. S., Rath, J. L., VandenBoer, T. C., Roberts, J. M., Brown, S. S., and Yalin, A.  
 654 P.: Cavity ring-down spectroscopy sensor for detection of hydrogen chloride, *Atmospheric Meas. Tech.*, 7, 345–  
 655 357, <https://doi.org/10.5194/amt-7-345-2014>, 2014.
- 656 Harris, G. W., Klemp, D., and Zenker, T.: An upper limit on the HCl near-surface mixing ratio over the Atlantic  
 657 measured using TDLAS, *J. Atmospheric Chem.*, 15, 327–332, <https://doi.org/10.1007/BF00115402>, 1992.
- 658 Haskins, J. D., Jaeglé, L., Shah, V., Lee, B. H., Lopez-Hilfiker, F. D., Campuzano-Jost, P., Schroder, J. C., Day,  
 659 D. A., Guo, H., Sullivan, A. P., Weber, R., Dibb, J., Campos, T., Jimenez, J. L., Brown, S. S., and Thornton, J.  
 660 A.: Wintertime Gas-Particle Partitioning and Speciation of Inorganic Chlorine in the Lower Troposphere Over  
 661 the Northeast United States and Coastal Ocean, *J. Geophys. Res. Atmospheres*, 123, 12,897–12,916,  
 662 <https://doi.org/10.1029/2018JD028786>, 2018.



- 663 Huffman, J. A., Docherty, K. S., Aiken, A. C., Cubison, M. J., Ulbrich, I. M., DeCarlo, P. F., Sueper, D., Jayne,  
664 J. T., Worsnop, D. R., Ziemann, P. J., and Jimenez, J. L.: Chemically-resolved aerosol volatility measurements  
665 from two megacity field studies, *Atmospheric Chem. Phys.*, 9, 7161–7182, [https://doi.org/10.5194/acp-9-7161-](https://doi.org/10.5194/acp-9-7161-2009)  
666 2009, 2009.
- 667 Jahn, L. G., Wang, D. S., Dhulipala, S. V., and Ruiz, L. H.: Gas-Phase Chlorine Radical Oxidation of Alkanes:  
668 Effects of Structural Branching, NO<sub>x</sub>, and Relative Humidity Observed during Environmental Chamber  
669 Experiments, *J. Phys. Chem. A*, 125, 7303–7317, <https://doi.org/10.1021/acs.jpca.1c03516>, 2021.
- 670 Keene, W. C., Khalil, M. A. K., Erickson, D. J., McCulloch, A., Graedel, T. E., Lobert, J. M., Aucott, M. L.,  
671 Gong, S. L., Harper, D. B., Kleiman, G., Midgley, P., Moore, R. M., Seuzaret, C., Sturges, W. T., Benkovitz, C.  
672 M., Koropalov, V., Barrie, L. A., and Li, Y. F.: Composite global emissions of reactive chlorine from  
673 anthropogenic and natural sources: Reactive Chlorine Emissions Inventory, *J. Geophys. Res. Atmospheres*, 104,  
674 8429–8440, <https://doi.org/10.1029/1998JD100084>, 1999.
- 675 Knipping, E. M., Lakin, M. J., Foster, K. L., Jungwirth, P., Tobias, D. J., Gerber, R. B., Dabdub, D., and Finlayson-  
676 Pitts, B. J.: Experiments and Simulations of Ion-Enhanced Interfacial Chemistry on Aqueous NaCl Aerosols,  
677 *Science*, 288, 301–306, <https://doi.org/10.1126/science.288.5464.301>, 2000.
- 678 Laasonen, K. E. and Klein, M. L.: Ab Initio Study of Aqueous Hydrochloric Acid, *J. Phys. Chem. A*, 101, 98–  
679 102, <https://doi.org/10.1021/jp962513r>, 1997.
- 680 Laskin, A., Moffet, R. C., Gilles, M. K., Fast, J. D., Zaveri, R. A., Wang, B., Nigge, P., and Shutthanandan, J.:  
681 Tropospheric chemistry of internally mixed sea salt and organic particles: Surprising reactivity of NaCl with weak  
682 organic acids, *J. Geophys. Res. Atmospheres*, 117, <https://doi.org/10.1029/2012JD017743>, 2012.
- 683 Lee, B. H., Lopez-Hilfiker, F. D., Schroder, J. C., Campuzano-Jost, P., Jimenez, J. L., McDuffie, E. E., Fibiger,  
684 D. L., Veres, P. R., Brown, S. S., Campos, T. L., Weinheimer, A. J., Flocke, F. F., Norris, G., O'Mara, K., Green,  
685 J. R., Fiddler, M. N., Bililign, S., Shah, V., Jaeglé, L., and Thornton, J. A.: Airborne Observations of Reactive  
686 Inorganic Chlorine and Bromine Species in the Exhaust of Coal-Fired Power Plants, *J. Geophys. Res.*  
687 *Atmospheres*, 123, 11,225–11,237, <https://doi.org/10.1029/2018JD029284>, 2018.
- 688 Li, G., Gordon, I. E., Bernath, P. F., and Rothman, L. S.: Direct fit of experimental ro-vibrational intensities to  
689 the dipole moment function: Application to HCl, *J. Quant. Spectrosc. Radiat. Transf.*, 112, 1543–1550,  
690 <https://doi.org/10.1016/j.jqsrt.2011.03.014>, 2011.
- 691 Liao, J., Huey, L. G., Liu, Z., Tanner, D. J., Cantrell, C. A., Orlando, J. J., Flocke, F. M., Shepson, P. B.,  
692 Weinheimer, A. J., Hall, S. R., Ullmann, K., Beine, H. J., Wang, Y., Ingall, E. D., Stephens, C. R., Hornbrook, R.  
693 S., Apel, E. C., Riemer, D., Fried, A., Mauldin III, R. L., Smith, J. N., Staebler, R. M., Neuman, J. A., and Nowak,  
694 J. B.: High levels of molecular chlorine in the Arctic atmosphere, *Nat. Geosci.*, 7, 91–94,  
695 <https://doi.org/10.1038/ngeo2046>, 2014.
- 696 Liu, X., Deming, B., Pagonis, D., Day, D. A., Palm, B. B., Talukdar, R., Roberts, J. M., Veres, P. R., Krechmer,  
697 J. E., Thornton, J. A., de Gouw, J. A., Ziemann, P. J., and Jimenez, J. L.: Effects of gas–wall interactions on  
698 measurements of semivolatile compounds and small polar molecules, *Atmospheric Meas. Tech.*, 12, 3137–3149,  
699 <https://doi.org/10.5194/amt-12-3137-2019>, 2019.
- 700 Marcy, T. P., Fahey, D. W., Gao, R. S., Popp, P. J., Richard, E. C., Thompson, T. L., Rosenlof, K. H., Ray, E. A.,  
701 Salawitch, R. J., Atherton, C. S., Bergmann, D. J., Ridley, B. A., Weinheimer, A. J., Loewenstein, M., Weinstock,



- 702 E. M., and Mahoney, M. J.: Quantifying Stratospheric Ozone in the Upper Troposphere with in Situ Measurements  
 703 of HCl, *Science*, 304, 261–265, <https://doi.org/10.1126/science.1093418>, 2004.
- 704 McCulloch, A., Aucott, M. L., Benkovitz, C. M., Graedel, T. E., Kleiman, G., Midgley, P. M., and Li, Y.-F.:  
 705 Global emissions of hydrogen chloride and chloromethane from coal combustion, incineration and industrial  
 706 activities: Reactive Chlorine Emissions Inventory, *J. Geophys. Res. Atmospheres*, 104, 8391–8403,  
 707 <https://doi.org/10.1029/1999JD900025>, 1999.
- 708 Neuman, J. A., Huey, L. G., Ryerson, T. B., and Fahey, D. W.: Study of Inlet Materials for Sampling Atmospheric  
 709 Nitric Acid, *Environ. Sci. Technol.*, 33, 1133–1136, <https://doi.org/10.1021/es980767f>, 1999.
- 710 Osthoff, H. D., Roberts, J. M., Ravishankara, A. R., Williams, E. J., Lerner, B. M., Sommariva, R., Bates, T. S.,  
 711 Coffman, D., Quinn, P. K., Dibb, J. E., Stark, H., Burkholder, J. B., Talukdar, R. K., Meagher, J., Fehsenfeld, F.  
 712 C., and Brown, S. S.: High levels of nitryl chloride in the polluted subtropical marine boundary layer, *Nat. Geosci.*,  
 713 1, 324–328, <https://doi.org/10.1038/ngeo177>, 2008.
- 714 Oum, K. W., Lakin, M. J., DeHaan, D. O., Brauers, T., and Finlayson-Pitts, B. J.: Formation of Molecular Chlorine  
 715 from the Photolysis of Ozone and Aqueous Sea-Salt Particles, *Science*, 279, 74–76,  
 716 <https://doi.org/10.1126/science.279.5347.74>, 1998.
- 717 Pollack, I. B., Lindaas, J., Roscioli, J. R., Agnese, M., Permar, W., Hu, L., and Fischer, E. V.: Evaluation of  
 718 ambient ammonia measurements from a research aircraft using a closed-path QC-TILDAS operated with active  
 719 continuous passivation, *Atmospheric Meas. Tech.*, 12, 3717–3742, <https://doi.org/10.5194/amt-12-3717-2019>,  
 720 2019.
- 721 Pszenny, A. A. P., Fischer, E. V., Russo, R. S., Sive, B. C., and Varner, R. K.: Estimates of Cl atom concentrations  
 722 and hydrocarbon kinetic reactivity in surface air at Appledore Island, Maine (USA), during International  
 723 Consortium for Atmospheric Research on Transport and Transformation/Chemistry of Halogens at the Isles of  
 724 Shoals, *J. Geophys. Res. Atmospheres*, 112, <https://doi.org/10.1029/2006JD007725>, 2007.
- 725 R Core Team: R: A language and environment for statistical computing., 2021.
- 726 Ren, X., Sun, R., Chi, H.-H., Meng, X., Li, Y., and Levendis, Y. A.: Hydrogen chloride emissions from  
 727 combustion of raw and torrefied biomass, *Fuel*, 200, 37–46, <https://doi.org/10.1016/j.fuel.2017.03.040>, 2017.
- 728 Roberts, J. M., Veres, P., Warneke, C., Neuman, J. A., Washenfelder, R. A., Brown, S. S., Baasandorj, M.,  
 729 Burkholder, J. B., Burling, I. R., Johnson, T. J., Yokelson, R. J., and de Gouw, J.: Measurement of HONO, HNCO,  
 730 and other inorganic acids by negative-ion proton-transfer chemical-ionization mass spectrometry (NI-PT-CIMS):  
 731 application to biomass burning emissions, *Atmospheric Meas. Tech.*, 3, 981–990, [https://doi.org/10.5194/amt-3-](https://doi.org/10.5194/amt-3-981-2010)  
 732 981-2010, 2010.
- 733 Roscioli, J. R., Zahniser, M. S., Nelson, D. D., Herndon, S. C., and Kolb, C. E.: New Approaches to Measuring  
 734 Sticky Molecules: Improvement of Instrumental Response Times Using Active Passivation, *J. Phys. Chem. A*,  
 735 120, 1347–1357, <https://doi.org/10.1021/acs.jpca.5b04395>, 2016.
- 736 RStudio Team: RStudio: Integrated Development Environment for R, 2021.
- 737 Saliba, N. A., Yang, H., and Finlayson-Pitts, B. J.: Reaction of Gaseous Nitric Oxide with Nitric Acid on Silica  
 738 Surfaces in the Presence of Water at Room Temperature, *J. Phys. Chem. A*, 105, 10339–10346,  
 739 <https://doi.org/10.1021/jp012330r>, 2001.
- 740 Scott, D. C., Herman, R. L., Webster, C. R., May, R. D., Flesch, G. J., and Moyer, E. J.: Airborne Laser Infrared  
 741 Absorption Spectrometer (ALIAS-II) for in situ atmospheric measurements of N<sub>2</sub>O, CH<sub>4</sub>, CO, HCL, and NO<sub>2</sub>



- 742 from balloon or remotely piloted aircraft platforms, *Appl. Opt.*, 38, 4609–4622,  
 743 <https://doi.org/10.1364/AO.38.004609>, 1999.
- 744 Simpson, W. R., Brown, S. S., Saiz-Lopez, A., Thornton, J. A., and von Glasow, R.: Tropospheric Halogen  
 745 Chemistry: Sources, Cycling, and Impacts, *Chem. Rev.*, 115, 4035–4062, <https://doi.org/10.1021/cr5006638>,  
 746 2015.
- 747 Singh, H. B., Gregory, G. L., Anderson, B., Browell, E., Sachse, G. W., Davis, D. D., Crawford, J., Bradshaw, J.  
 748 D., Talbot, R., Blake, D. R., Thornton, D., Newell, R., and Merrill, J.: Low ozone in the marine boundary layer of  
 749 the tropical Pacific Ocean: Photochemical loss, chlorine atoms, and entrainment, *J. Geophys. Res. Atmospheres*,  
 750 101, 1907–1917, <https://doi.org/10.1029/95JD01028>, 1996.
- 751 Sumner, A. L., Menke, E. J., Dubowski, Y., Newberg, J. T., Penner, R. M., Hemminger, J. C., Wingen, L. M.,  
 752 Brauers, T., and Finlayson-Pitts, B. J.: The nature of water on surfaces of laboratory systems and implications for  
 753 heterogeneous chemistry in the troposphere, *Phys. Chem. Chem. Phys.*, 6, 604–613,  
 754 <https://doi.org/10.1039/B308125G>, 2004.
- 755 Tao, Y., VandenBoer, T. C., Veres, P. R., Warneke, C., de Gouw, J. A., Weber, R. J., Markovic, M. Z., Zhao, Y.,  
 756 Baker, K. R., Kelly, J. T., Murphy, J. G., Young, C. J., and Roberts, J. M.: Hydrogen Chloride (HCl) at Ground  
 757 Sites During CalNex 2010 and Insight Into Its Thermodynamic Properties, *J. Geophys. Res. Atmospheres*, 127,  
 758 e2021JD036062, <https://doi.org/10.1029/2021JD036062>, 2022.
- 759 Toth, R. A., Hunt, R. H., and Plyler, E. K.: Line strengths, line widths, and dipole moment function for HCl, *J.*  
 760 *Mol. Spectrosc.*, 35, 110–126, [https://doi.org/10.1016/0022-2852\(70\)90169-4](https://doi.org/10.1016/0022-2852(70)90169-4), 1970.
- 761 Tuckermann, M., Ackermann, R., Götz, C., Lorenzen-Schmidt, H., Senne, T., Stutz, J., Trost, B., Unold, W., and  
 762 Platt, U.: DOAS-observation of halogen radical-catalysed arctic boundary layer ozone destruction during the  
 763 ARCTOC-campaigns 1995 and 1996 in Ny-Ålesund, Spitsbergen, *Tellus B Chem. Phys. Meteorol.*, 49, 533–555,  
 764 <https://doi.org/10.3402/tellusb.v49i5.16005>, 1997.
- 765 Veres, P., Roberts, J. M., Warneke, C., Welsh-Bon, D., Zahniser, M., Herndon, S., Fall, R., and de Gouw, J.:  
 766 Development of negative-ion proton-transfer chemical-ionization mass spectrometry (NI-PT-CIMS) for the  
 767 measurement of gas-phase organic acids in the atmosphere, *Int. J. Mass Spectrom.*, 274, 48–55,  
 768 <https://doi.org/10.1016/j.ijms.2008.04.032>, 2008.
- 769 Wang, X., Jacob, D. J., Eastham, S. D., Sulprizio, M. P., Zhu, L., Chen, Q., Alexander, B., Sherwen, T., Evans,  
 770 M. J., Lee, B. H., Haskins, J. D., Lopez-Hilfiker, F. D., Thornton, J. A., Huey, G. L., and Liao, H.: The role of  
 771 chlorine in global tropospheric chemistry, *Atmospheric Chem. Phys.*, 19, 3981–4003, [https://doi.org/10.5194/acp-](https://doi.org/10.5194/acp-19-3981-2019)  
 772 19-3981-2019, 2019.
- 773 Wang, X., Jacob, D. J., Downs, W., Zhai, S., Zhu, L., Shah, V., Holmes, C. D., Sherwen, T., Alexander, B., Evans,  
 774 M. J., Eastham, S. D., Neuman, J. A., Veres, P. R., Koenig, T. K., Volkamer, R., Huey, L. G., Bannan, T. J.,  
 775 Percival, C. J., Lee, B. H., and Thornton, J. A.: Global tropospheric halogen (Cl, Br, I) chemistry and its impact  
 776 on oxidants, *Atmospheric Chem. Phys.*, 21, 13973–13996, <https://doi.org/10.5194/acp-21-13973-2021>, 2021.
- 777 Watson, N.: Ammonia and Water Abundance Measurements from Los Gatos Research Ammonia Analyzer  
 778 Instrument at Manchester Air Quality Site 2019–22, NERC EDS Cent. Environ. Data Anal.,  
 779 <https://catalogue.ceda.ac.uk/uuid/5fc811f707f54415b129882a38889501>, 2022a.



- 780 Watson, N.: Nitrogen Dioxide Abundance Data from Teledyne Model T500U Instrument at the Manchester Air  
 781 Quality Site, NERC EDS Cent. Environ. Data Anal.,  
 782 <https://catalogue.ceda.ac.uk/uuid/f60761f3279042859e5c2902dfa0f2ef>, 2022b.
- 783 Watson, N.: NO and NO<sub>y</sub> Abundance Data from Thermo Model 42i-Y NOY Analyzer Instrument at the  
 784 Manchester Air Quality Site, NERC EDS Cent. Environ. Data Anal.,  
 785 <https://catalogue.ceda.ac.uk/uuid/1d58f2f5e7874e55a83ca57311dcfb9a>, 2022c.
- 786 Webster, C. R., May, R. D., Trimble, C. A., Chave, R. G., and Kendall, J.: Aircraft (ER-2) laser infrared absorption  
 787 spectrometer (ALIAS) for in-situ stratospheric measurements of HCl, N<sub>2</sub>O, CH<sub>4</sub>, NO<sub>2</sub>, and HNO<sub>3</sub>, Appl. Opt., 33,  
 788 454–472, <https://doi.org/10.1364/AO.33.000454>, 1994.
- 789 Wilkerson, J., Sayres, D. S., Smith, J. B., Allen, N., Rivero, M., Greenberg, M., Martin, T., and Anderson, J. G.:  
 790 In situ observations of stratospheric HCl using three-mirror integrated cavity output spectroscopy, Atmospheric  
 791 Meas. Tech. Discuss., 1–38, <https://doi.org/10.5194/amt-2021-6>, 2021.
- 792 Wingenter, O. W., Kubo, M. K., Blake, N. J., Smith Jr., T. W., Blake, D. R., and Rowland, F. S.: Hydrocarbon  
 793 and halocarbon measurements as photochemical and dynamical indicators of atmospheric hydroxyl, atomic  
 794 chlorine, and vertical mixing obtained during Lagrangian flights, J. Geophys. Res. Atmospheres, 101, 4331–4340,  
 795 <https://doi.org/10.1029/95JD02457>, 1996.
- 796 Yokelson, R. J., Christian, T. J., Bertschi, I. T., and Hao, W. M.: Evaluation of adsorption effects on measurements  
 797 of ammonia, acetic acid, and methanol, J. Geophys. Res. Atmospheres, 108,  
 798 <https://doi.org/10.1029/2003JD003549>, 2003.
- 799 Zahniser, M. S., Nelson, D. D., McManus, B., Keabian, P. L., and Lloyd, D.: Measurement of trace gas fluxes  
 800 using tunable diode laser spectroscopy, Philos. Trans. R. Soc. Lond. Ser. Phys. Eng. Sci., 351, 371–382,  
 801 <https://doi.org/10.1098/rsta.1995.0040>, 1995.
- 802 Zhang, B., Shen, H., Yun, X., Zhong, Q., Henderson, B. H., Wang, X., Shi, L., Gunthe, S. S., Huey, L. G., Tao,  
 803 S., Russell, A. G., and Liu, P.: Global Emissions of Hydrogen Chloride and Particulate Chloride from Continental  
 804 Sources, Environ. Sci. Technol., 56, 3894–3904, <https://doi.org/10.1021/acs.est.1c05634>, 2022.
- 805